

DETERMINATION OF ELASTIC PROPERTIES OF POLYMER
NANOCOMPOSITES USING EMBEDDED ELEMENT METHOD

A THESIS SUBMITTED TO
THE GRADUATE SCHOOL OF NATURAL AND APPLIED SCIENCES
OF
MIDDLE EAST TECHNICAL UNIVERSITY

BY

AYSU ELİF ALTAY

IN PARTIAL FULFILLMENT OF THE REQUIREMENTS
FOR
THE DEGREE OF MASTER OF SCIENCE
IN
AEROSPACE ENGINEERING

FEBRUARY 2022

Approval of the thesis:

**DETERMINATION OF ELASTIC PROPERTIES OF POLYMER
NANOCOMPOSITES USING EMBEDDED ELEMENT METHOD**

submitted by **AYSU ELİF ALTAY** in partial fulfillment of the requirements for the degree of **Master of Science in Aerospace Engineering, Middle East Technical University** by,

Prof. Dr. Halil Kalıpçılar
Dean, Graduate School of **Natural and Applied Sciences** _____

Prof. Dr. Serkan Özgen
Head of the Department, **Aerospace Engineering** _____

Assoc. Prof. Dr. Ercan Gürses
Supervisor, **Aerospace Engineering Department, METU** _____

Examining Committee Members:

Prof. Dr. Altan Kayran
Aerospace Engineering Department, METU _____

Assoc. Prof. Dr. Ercan Gürses
Aerospace Engineering Department, METU _____

Prof. Prof. Dr. Demirkan Çöker
Aerospace Engineering Department, METU _____

Assoc. Prof. Dr. Melin Şahin
Aerospace Engineering Department, METU _____

Assoc. Prof. Dr. Barış Sabuncuoğlu
Mechanical Engineering Department, Hacettepe University _____

Date: 11.02.2022

I hereby declare that all information in this document has been obtained and presented in accordance with academic rules and ethical conduct. I also declare that, as required by these rules and conduct, I have fully cited and referenced all material and results that are not original to this work.

Name, Last name : Aysu Elif Altay

Signature :

ABSTRACT

DETERMINATION OF ELASTIC PROPERTIES OF POLYMER NANOCOMPOSITES USING EMBEDDED ELEMENT METHOD

Altay, Aysu Elif
Master of Science, Aerospace Engineering
Supervisor : Assoc.Prof. Dr. Ercan Gürses

February 2022, 98 pages

Composites are preferred in different industries due to their high strength and lightness. Carbon nanotube (CNT) reinforced polymer composites are preferred composites due to their superior mechanical properties. CNTs in the material increase the stiffness of the structure positively, but the presence of CNTs makes the structure heterogeneous. The objective of this study is to determine the effective elastic properties of polymer nanocomposites using the embedded element method. Due to their nanosize, finite element analysis of CNT reinforced polymer nanocomposites requires high computation power. In the embedded element method, the finite element mesh of the CNTs and the matrix do not need to be compatible, which provides convenience in modeling. Hence, the embedded element method, which is one of the modeling techniques of the Abaqus software, is selected in this study. Representative Volume Elements (RVEs) are generated, and computational homogenization analyses are conducted using the embedded element method. The results of the conventional finite element method and the embedded element method are compared. Since a single CNT in the heterogeneous structure does not accurately represent reality, models containing randomly-placed and randomly-oriented CNTs are created. The effect of small aggregation on the homogenization process is studied

since CNTs tend to agglomerate due to their inherent nature. Finally, the number of minimum CNTs required in computational homogenization is determined by a numerical convergence study. Commercial finite element program Abaqus is used for all analyses in this study, and Python software is utilized to compute homogenized properties and generate RVEs.

Keywords: Finite Element Analysis, Composites, Embedded Element Method, Representative Volume Element, Carbon Nanotube

ÖZ

GÖMÜLÜ ELEMAN YÖNTEMİ KULLANILARAK POLİMER NANOKOMPOZİTLERİN ELASTİK ÖZELLİKLERİNİN BELİRLENMESİ

Altay, Aysu Elif
Yüksek Lisans, Havacılık ve Uzay Mühendisliği
Tez Yöneticisi: Doç. Dr. Ercan Gürses

Şubat 2022, 98 sayfa

Kompozitler yüksek dayanım ve hafif olmaları nedeniyle değişik endüstrilerde tercih edilmektedir. Karbon nanotüp (KNT) ile güçlendirilmiş polimer kompozitler de yapıya sağladıkları avantajlar sebebiyle tercih edilen kompozitlerden bir tanesidir. Malzemedeki KNTler yapı dayanımını olumlu yönde arttırmaktadır, fakat KNTlerin varlığı yapıyı heterojen hale getirmektedir. Bu çalışmanın temel amacı, gömülü eleman yöntemini kullanarak polimer nanokompozitlerin elastik özelliklerinin belirlenmesidir. KNTlerin nano boyutta olması, KNT içeren kompozit analizleri için yüksek bilgisayar gücü gerektirir. Gömülü eleman yönteminde KNTlerin düğüm noktası ile matris düğüm noktasının çakışması gerekmemektedir, bu da modellemede kolaylık sağlamaktadır. Bu yüzden Abaqus programının modelleme tekniklerinden biri olan gömülü eleman yöntemi kullanılmıştır. Malzemeden alınan Temsili Hacim Elemanı (THE) kullanılarak hesaplamalı homojenizasyon analizleri yapılmıştır. Geleneksel sonlu elemanlar yöntemi ile gömülü eleman yönteminin sonuçları karşılaştırılmıştır. Heterojen yapı içerisinde bulunan tek bir KNT tüm modeli tam olarak temsil etmediğinden, rastgele yerleştirilmiş ve rastgele yönlendirilmiş KNT içeren modeller oluşturulmuştur. KNTler yapıları nedeniyle kümelenme eğiliminde olduklarından, oluşabilecek küçük kümelenmenin

homojenleřtirme iřlemi zerindeki etkisi incelenmiřtir. Son olarak, sayısal bir yakınsama alıřması ile hesaplamalı homojenleřtirme iin gereken minimum KNT sayısı belirlenmiřtir. Bu alıřmadaki tm analizler iin Abaqus programı kullanılmıřtır. Homojenleřtirme, model oluřturma ve rastgelelik gibi iřlemler iin ise Python yazılımından yararlanılmıřtır.

Anahtar Kelimeler: Sonlu Eleman Analizi, Kompozit, Gml Eleman Yntemi, Temsili Hacim Elemanı, Karbon Nanotp

To My Mom

ACKNOWLEDGMENTS

I would like to express my sincere appreciation to my supervisor Assoc. Prof. Dr. Ercan Gürses for his guidance, helpful advice, and encouragement throughout the research.

I also would like to thank my colleagues Çağatay Koyuncuoğlu and Mert Tokel for helpful discussions about my thesis.

My deepest gratitude to my beloved mom; I give my special thanks to my amazing mom Serpil for her endless love, patience, encouragement, and unconditional support throughout my life.

TABLE OF CONTENTS

ABSTRACT.....	v
ÖZ.....	vii
ACKNOWLEDGMENTS	x
TABLE OF CONTENTS.....	xi
LIST OF TABLES	xiv
LIST OF FIGURES	xvii
LIST OF ABBREVIATIONS.....	xix
LIST OF SYMBOLS	xx
CHAPTERS	
1 INTRODUCTION	1
1.1 Overview	1
1.2 Motivation	3
1.3 Objective	3
1.4 Literature Review	4
1.4.1 Representative Volume Element.....	4
1.4.2 Embedded Element Method.....	6
1.5 Outline.....	8
2 METHOD OF APPROACH.....	9
2.1 Representative Volume Element (RVE)	9
2.2 Embedded Element Method	11

2.3	Homogenization Procedure.....	14
2.3.1	Averaging	16
2.3.2	Stiffness and Compliance Matrices	20
2.3.3	Boundary Conditions.....	25
2.4	Random Sequential Adsorption Algorithm	26
2.5	Rule of Mixtures	31
3	VALIDATION STUDIES.....	33
3.1	Mesh Convergence Study	33
3.2	Effects of RVE Shapes	36
3.3	Effect of Fiber Placement	39
3.4	Embedded and Partitioned Models	41
3.5	Validation with Literature.....	46
4	HOMOGENIZATION OF ELASTIC PROPERTIES OF CARBON NANOTUBE POLYMER COMPOSITES	51
4.1	Randomly Distributed Unidirectional Aligned CNTs	51
4.2	Randomly Distributed CNTs	55
4.3	The Effect of Number of Randomly Oriented CNTs	61
4.4	The Effect of Clustering on the Elastic Properties	68
5	CONCLUSION AND FUTURE WORK.....	75
	REFERENCES	77
	APPENDICES	
A.	Sample Python Code for Averaging Calculations	83
B.	Randomly Selected Cubes for CNT Placement.....	93
C.	Python Code for Randomly Selected Angles	95

D.	3x3 Cluster Model Results for 2% and 3% Volume Fraction.....	97
----	--	----

LIST OF TABLES

TABLES

Table 2.1 Random fiber generation methods, their related volume fractions and aspect ratios	28
Table 3.1 Mesh quality parameters	33
Table 3.2 Elastic modulus results of mesh quality study	34
Table 3.3 Shear modulus results of mesh quality study	34
Table 3.4 Poisson's Ratio results of mesh quality study	34
Table 3.5 Dimension of samples [nm]	36
Table 3.6 Mechanical properties of fiber and matrix	36
Table 3.7 Elastic Modulus results of different RVE shapes.....	38
Table 3.8 Shear Modulus results of different RVE shapes	38
Table 3.9 Poisson's Ratio results of different RVE shapes.....	38
Table 3.10 Percentage differences of material constants of different RVE shapes with the average values.	38
Table 3.11 Model dimensions	39
Table 3.12 Elastic property results of CNT throughout RVE and CNT embedded into RVE.....	41
Table 3.13 Homogenized elastic properties for the partitioned model and the embedded model.....	42
Table 3.14 Reduced elastic modulus properties for CNT	43
Table 3.15 Homogenized elastic properties for the partitioned model and the embedded model with reduced Young's modulus of CNT	43
Table 3.16 Homogenized elastic properties for the partitioned and the embedded models for CNT completely placed inside matrix.....	45
Table 3.17 Homogenized elastic properties for the partitioned and the embedded models with reduced Young's modulus for CNT completely placed inside matrix	46
Table 3.18 Elastic constants of the materials	47

Table 3.19 The number of mesh seeds for fiber according to fiber diameter	48
Table 3.20 Results of Liu [47] digitized by WebPlotDigitizer [48]	48
Table 3.21 Reanalyze result of the longitudinal elastic modulus for the traditional(partitioned) model and the embedded model	49
Table 3.22 Reanalyze results of the transverse elastic modulus	50
Table 4.1 Model dimensions for randomly distributed unidirectional CNTs	52
Table 4.2 Material properties of the model.....	52
Table 4.3 Number of elements for 1% and 3% models	54
Table 4.4 Homogenized elastic properties of aligned CNTs for 1% and 3% volume fractions.....	54
Table 4.5 Number of fibers according to the volume fractions	56
Table 4.6 Elastic properties for 1% randomly distributed CNTs.....	58
Table 4.7 Elastic properties for 2% randomly distributed CNTs.....	58
Table 4.8 Elastic properties for 3% randomly distributed CNTs.....	59
Table 4.9 Average elastic properties and the maximum differences for 1% randomly distributed CNTs.....	60
Table 4.10 Average elastic properties and the maximum differences for 2% randomly distributed CNTs.....	60
Table 4.11 Average elastic properties and the maximum differences for 3% randomly distributed CNTs.....	61
Table 4.12 Homogenized elastic properties for five different 3×3 cluster models with volume fraction of 1%	71
Table 4.13 Homogenized elastic properties for five different 4×4 cluster models with volume fraction of 1%	71
Table 4.14 Homogenized elastic properties for five different 5×5 cluster models with volume fraction of 1%	72
Table 4.15 Percentage difference between cluster models and the random model (no cluster) results.....	73
Table 5.1 Homogenized elastic properties for five different 3x3 cluster models with volume fraction of 2%	97

Table 5.2 Homogenized elastic properties for five different 3x3 cluster models with volume fraction of 3%	98
Table 5.3 Comparison of elastic and shear modulus with changing volume fraction for random and 3x3 cluster model.....	98

LIST OF FIGURES

FIGURES

Figure 1.1 Overview of SWCNT and MWCNT [2]	2
Figure 2.1 Different shapes of RVE	10
Figure 2.2 Illustration of Embedded and Host Regions.....	12
Figure 2.3 Representation of Nodes of Embedded and Host Element	13
Figure 2.4 Homogenization Procedure	14
Figure 2.5 Integrations points (a)(b) for fully integrated elements, (c)(d) with reduced integration elements [23].....	17
Figure 2.6 Representation of boundary conditions for three tensile a) ϵ_1 , b) ϵ_2 , c) ϵ_3 , and three shear d) ϵ_4 , e) ϵ_5 , f) ϵ_6 load cases	26
Figure 2.7 Main idea of the creating and placing fibers according to Modified RSA Algorithm [43]	29
Figure 2.8 Modified RSA Algorithm Flow Chart [43]	30
Figure 2.9 Voigt and Reuss model representation [44]	31
Figure 3.1 Models for (a) coarse, (b) normal and (c) fine meshes.....	34
Figure 3.2 E_1 , E_2 , and E_3 values for different mesh sizes (from coarse to fine).....	35
Figure 3.3 G_{12} , G_{13} , and G_{23} values for different mesh sizes (from coarse to fine). 35	35
Figure 3.4 Representation of CNT and matrix a) fiber shape (same for all samples) b) cylindrical c) hexagon d) rectangular shape of RVE.....	37
Figure 3.5 The model where the CNT is completely embedded into RVE	40
Figure 3.6 The model where the CNT is throughout RVE	40
Figure 3.7 Modeling embedded and host regions in Abaqus.....	42
Figure 3.8 Embedded model for CNT inside of the matrix	44
Figure 3.9 Dimensions of the model according to the article	47
Figure 4.1 RVE with 1% randomly distributed unidirectional CNTs a) general view b) front view c) side view d) CNTs only view.....	53
Figure 4.2 Division of the matrix into regular cubes	56

Figure 4.3 RVEs with randomly oriented CNTs for different volume fractions (a) 1%, (b) 2%, (c) 3%.....	57
Figure 4.4 Sample models for different number of CNTs a) 1, b) 10, c) 50, d) 100, e) 200, f) 400 CNTs. The volume fraction is 1% in all models.....	62
Figure 4.5 Average Elastic Modulus vs Number of CNTs for 1% volume fraction	64
Figure 4.6 Average shear modulus vs number of CNTs for 1% volume fraction...	64
Figure 4.7 The mean percentage difference for elastic modulus for different number of CNTs	66
Figure 4.8 The mean percentage difference for shear modulus for different number of CNTs	66
Figure 4.9 The worst percentage difference for elastic modulus for different number of CNTs	67
Figure 4.10 The worst percentage difference for shear modulus for different number of CNTs	68
Figure 4.11 3×3 Cluster model sample for 1% volume fraction a) side view of CNTs, b) iso view of CNTs, c) whole model	69
Figure 4.12 4×4 Cluster model sample for 1% volume fraction a) side view of CNTs, b) iso view of CNTs, c) whole model	69
Figure 4.13 5×5 Cluster model sample for 1% volume fraction a) side view of CNTs, b) iso view of CNTs, c) whole model	70

LIST OF ABBREVIATIONS

ABBREVIATIONS

AR	Aspect Ratio
avg	Average
CNT	Carbon Nano Tube
CNTRC	Carbon Nano Tube Reinforced Composite
DWCNT	Double-Walled Carbon Nano Tube
dof	Degree of Freedom
EE	Embedded Element
FE	Finite Element
FEA	Finite Element Analysis
FEM	Finite Element Method
IVOL	Integration Point Volume
PBC	Periodic Boundary Conditions
PEEK	Polyether Ether Ketone
RSA	Random Sequential Adsorption
RVE	Representative Volume Element
ROM	Rule of Mixtures
SWCNT	Single-Walled Carbon Nano Tube
MD	Molecular Dynamics
MPD	Mean Percentage Difference
MWCNT	Multi-Walled Carbon Nano Tube
V_f	Volume fraction
WPD	The Worst Percentage Difference

LIST OF SYMBOLS

SYMBOLS

σ	Stress
ε	Strain
ν	Poisson's Ratio
V_f	Volume Fraction
S	Stiffness Matrix
C	Compliance Matrix
$\bar{\sigma}$	Homogenized Stress Tensor
$\bar{\varepsilon}$	Homogenized Strain Tensor
\bar{E}	Average Elastic Modulus
\bar{G}	Average Shear Modulus
ΔE	Difference in Elastic Modulus
ΔG	Difference in Shear Modulus

CHAPTER 1

INTRODUCTION

1.1 Overview

Composite materials are widely used in different industries such as aerospace, automotive, marine, construction, electrical components. Effectivity of the composite structures is promising for future technology. Composite structures are made of two or more materials to produce new material with better quality. They utilize desired properties of each subcomponent such as improved strength, stiffness, lightweight, conductivity, thermal resistance, ultraviolet sustainability. Composites are comprised of matrix and reinforcement material. Both of these subcomponents have different advantages. For instance, the matrix material provides lightweight, and reinforcement supplies strength. If they are used separately, the matrix material is not enough in terms of strength, and reinforcement does not provide lightweight. By including reinforcement in a matrix, both of the properties are utilized.

In structural components, generally, fiber-reinforced composites are used. Fiber-reinforced composites usually have thermoplastic or thermoset matrices. Carbon, glass, or aramid fiber is used as a reinforcement material. Reinforcement materials can be aligned through the entire matrix. Matrix and reinforcement decide the general characteristic of the composites. At this point, carbon nanotubes are superior reinforcement materials used in composite structures. Carbon nanotubes (CNT) are highly stiff materials, and they provide lightweight. Their diameter to length ratio changes from 5 to 10^6 . This property provides excessive strength in the fiber length direction. In 1991, Iijima discovered this promising material [1].

CNTs are basically rolled-up graphene sheets. They are allotropes of carbon, and their diameter dimensions are in nanometers. They exhibit unusual mechanical and electronic properties such as extraordinary strength, high aspect ratio, lightweight, fast electron transfer, and semiconducting characteristic. They are classified according to the number of walls they have. These are single-walled CNTs (SWCNT), double-walled CNTs (DWCNT) and multi-walled CNTs (MWCNT). SWCNT, and MWCNT can be seen in Figure 1.1.

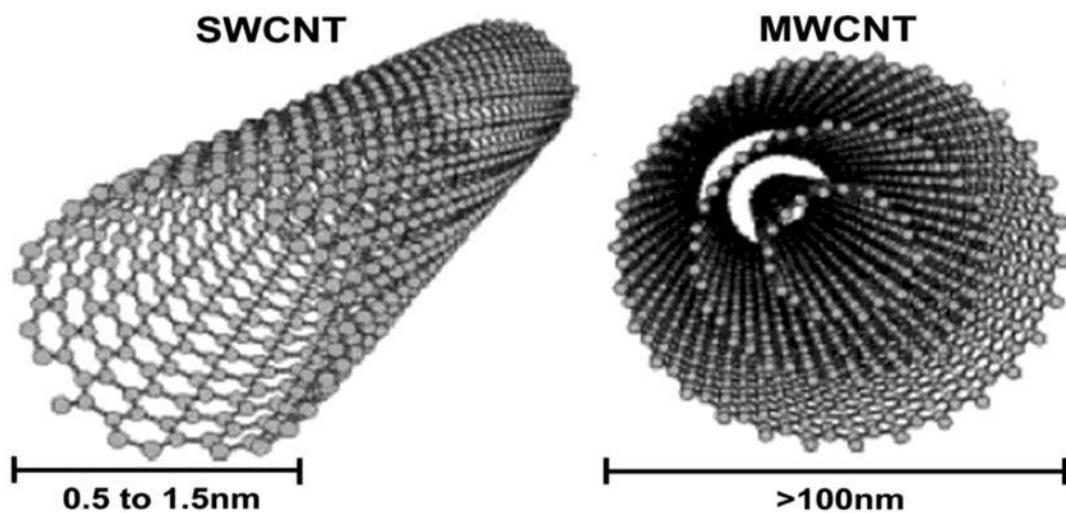


Figure 1.1 Overview of SWCNT and MWCNT [2]

In different fields of technology, CNT reinforced composites are used to utilize their superior properties. For example, The Boeing Company has a patent related to the use of CNT for structural health monitoring. It is stated that structural defects can be detected by the piezoresistivity of CNT [3]. In marine technology, Zyvex Technologies produced a boat called *Piranha Unmanned Surface Vessel*, built from CNT reinforced composite. Also, they are in cooperation with Easton Sports for CNT enhanced products in sports such as baseball bats [4][5]. Considering the features of CNT, these examples show that CNTs will have an influence on future technology in many fields.

1.2 Motivation

It can be seen that CNT reinforced composites will be used in different fields of technology in the future. If we focus on the structural advantages of CNT, they provide extraordinary stiffness and are lightweight at the same time. This is one of the most desired design criteria for a structure. To be able to use this nanomaterial in the industry, it is necessary to comprehend how a material reacts under different load cases. Unknown mechanical properties do not satisfy safety requirements, and that makes material out of favor. This means that one needs to focus on mechanical properties.

The synthesis of CNT material can be made in different ways: arc-discharge synthesis, laser ablation and chemical vapor deposition [6]. Unidirectional aligning of CNT in the matrix is hard to produce since they have a high aspect ratio and agglomeration tendency [7]. Instead, CNTs can be used to strengthen the structure by adding them as chopped. Chopped CNT materials make composite heterogeneous, and unlike homogeneous materials, it is more complicated to decide its mechanical properties. The heterogeneous structure of CNT reinforced composites is the starting point of this study. A proper approach is needed to determine the mechanical properties of these composites. The motivation of the study is to find a reliable, effective, and handy way for finite element analysis of CNT reinforced composites.

1.3 Objective

Mechanical properties of the isotropic and homogeneous materials are easier to determine, and these materials are more straightforward to analyze. However, this is not the case for heterogeneous materials. Chopped CNTs are dispersed in the matrix, and dispersion makes them heterogeneous. Average mechanical properties can be used to analyze this heterogeneous material.

In this study, the average mechanical properties of the CNT reinforced composites are studied. To this end, various representative volume elements (RVEs) are considered. Then a computational homogenization procedure is performed using different RVEs. The random sequential adsorption (RSA) method is used for CNT distribution in a matrix [8]. The embedded element (EE) method is used to ease these calculations. Simulia Abaqus/CAE software is chosen for finite element analysis (FEA), and Python programming language is mainly preferred for RVE generation and post-processing calculations.

In summary, the main objective of this study is the computational homogenization of the CNT reinforced composites and to find reliable mechanical properties by using the EE method.

1.4 Literature Review

1.4.1 Representative Volume Element

There are various studies for the analysis of heterogeneous materials in the literature. Components of heterogeneous material should be analyzed first to understand the material behavior. Previously, CNT composites were modeled based on molecular dynamics by many researchers. However, MD simulations have some restrictions, such as complex formulations, computational effort, and a huge number of atoms [9]. As an alternative, an RVE, a small portion of the heterogeneous material, can be considered to represent the entire composite material. RVE properties are significant for homogenization. The RVE shape, the RVE size, the number and placement of fibers should be chosen wisely. For this reason, different shapes of RVE should be checked. In [10], three different possibilities, square, cylindrical and hexagonal RVEs, were chosen to find effective mechanical properties. It was stated that cylindrical RVEs are in a tendency to overestimate the mechanical properties. Also, it was reported that a small amount of CNT addition (1% by weight) causes stiffness to increase between 36% to 42% [10]. Another concern is how to construct the

components of the RVE model. Hu et al. [11] constructed fibers as beam elements. In addition to that, 3D eight-noded brick element was suggested for modeling of inclusion so that consistency of the results could be achieved.

Odegard et al. [12] took advantage of the RVE model for CNT reinforced composites. They checked the effect of different orientations and concentrations. They observed that aligned fibers gave more stiffness to the structure compared to the random distribution. Also, increasing concentration (from 0% to 1%) provided increasing stiffness in material properties in their study.

Liu et al. [13] proposed an RVE model to evaluate the mechanical properties of CNTs. Three different load cases which depend on elasticity theory were suggested for analysis. They studied different volume fractions and lengths (short and long) of CNTs to examine the difference. They also claimed that RVE model results are compatible with experimental results.

Chen et al. [10] studied three different RVEs to comprehend the RVE shape effect. In addition to this, short and long fibers were considered. Short CNTs refer to the CNTs which are embedded in the matrix, and long CNTs are placed along the whole length of the RVE. In the article, axial and lateral uniform loads were applied as boundary conditions to achieve effective material properties. It is stated that both short and long CNTs showed reliable results compared with the rule of mixtures results.

To generalize RVE properties to the whole structure, Hu et al. [14] suggested utilizing the average results of several RVEs. Similarly, they applied three different loads to reach effective properties. Thereafter, RVE was divided into small cubics to place fibers inside the matrix. They used the Monte Carlo method to provide randomness of the fibers. Results of randomly oriented fibers were compared with experimental data, which validated the proposal.

In literature, RVE models are considered a reasonable starting point for the characterization of heterogeneous materials.

1.4.2 Embedded Element Method

Commonly, fiber and matrix are modeled separately, and parts are run together. This is a conventional way that is handy for analyzing a few parts. As the model gets more complex and has many parts, this approach will be challenging to follow. Thereupon, the embedded element method is an alternative way to ease modeling and meshing.

In classical FE analysis, all the nodes on the surface separating two parts should be mutual to elements of both parts. In the embedded element method, parts can be meshed separately and do not need to have mutual nodes (For detailed information about the EE method, please check Section 2.2). It enables to model matrix and fiber individually, which is very helpful when a large number of components exists.

If a significant number of CNTs are chopped and dispersed in the matrix. Then, modeling of every CNT would be time-wasting and effortful work. Analysis can be performed faster and easier by using the EE method. Due to its effectiveness and ease of application, many researchers have studied the EE method.

Lu et al. [15] applied the EE method to fiber-reinforced silica aerogel composites. Assuming that the interaction between matrix and fiber is zero, they simplified fibers and modeled them as a 1D element. They implemented the EE method to provide a connection between 1D element fibers and 3D element matrix. They found that the previous experimental results and their studies are comparable. However, they realized that the EE method causes extra stiffness in the model. To modify the EE method, they proposed to extract the elastic modulus of the matrix from the elastic modulus of fiber. Results showed that modification on elastic modulus leads to better results [16].

EE method was also used in biomechanics. Awasthi et al. [17] analyzed the structure of bone, thinking that bone is a kind of composite which is comprised of microfibril, tropocollagen, and organic matrix. Microfibril and tropocollagen were modeled as long fiber and spherical inclusion, respectively. EE method was applied to the bone structure to find homogenized values of the mechanical properties. It was also

emphasized that the EE method reduces the total number of degrees of freedom of the whole system, which results in reduced calculation time.

EE method has some restrictions as well. Matveeva et al. [18] explained these limitations in their study. One has to pay attention to mesh sizes in the host and the embedded regions since it affects the calculation mechanism of the EE method. The mesh size of the host region should be greater than the embedded region. The reason is that every node of embedded region should be inside the host region. Furthermore, the extra artificial stiffness caused by the EE method was noted in [18].

Song et al. [19] conducted a study to compare three methods: the rule of mixtures, the inclusion theory, and the FEM. The rule of mixtures is a well-known method to predict the mechanical properties of composites. The inclusion theory is based on strain concentration tensors. In the FEM model, the EE method is used to utilize its advantages. According to test data, FEM results are found to be closer to the experimental results.

EE method was also utilized to understand stress distribution on hybrid composites by Romanov [19]. Computation time and cost are limited to analyzing CNT modified fiber-reinforced composites. Hence, the EE method was implemented to analyze complex 3D geometries. He also stated that 1D beam elements were not preferred for modeling CNTs due to insufficient integration points. In addition, it was indicated that beam elements are not sufficient to show mechanical properties in the transverse directions.

To summarize, it can be concluded that the EE method is a commonly-used method due to its effectiveness, simplicity in meshing, and time-saving property. The EE method is applied, especially in complex models such as short fiber-reinforced composites. However, it is also taken into consideration that embedded elements cause additional stiffness, which can result an overestimated outcome. Therefore, extraction of the elastic modulus of the embedded region should be carried out.

1.5 Outline

This chapter gives brief information about this study. CNTs and their importance in the industry are emphasized. The motivation of the study is explained. The primary approach to the problem and suggested solution ways are described. A literature review is presented.

In the second chapter, the method of approach is presented. Firstly, the definition of RVE and its use are explained. After that comparison of the EE method and traditional partition method is shown. The homogenization procedure for heterogeneous materials is explained. The random sequential adsorption (RSA) method algorithm is explained for the random distribution of CNT. Rule of mixture is briefly reminded.

In the third chapter, different shapes of RVEs are compared. According to the results, the proper RVE shape is decided. A mesh convergence study is conducted to determine the element size. Different fiber placements (CNT along the matrix and CNT embedded in the matrix) are studied. Finally, a similar study is reperformed, and their results are compared.

In the fourth chapter, RVEs with many CNTs are studied. Randomly oriented fibers with different volume fractions are analyzed. Since there is randomness, different random samples are considered. The number of minimum CNTs required in computational homogenization is determined by a numerical convergence study. Finally, the effect of agglomeration on numerical homogenization is studied.

In the fifth chapter, the conclusions and future works are given.

CHAPTER 2

METHOD OF APPROACH

This chapter explains the concept of the representative volume element, the embedded element method, the homogenization procedure followed, and the random sequential adsorption algorithm.

2.1 Representative Volume Element (RVE)

Representative Volume Element (RVE) is the smallest element taken from a material, which shows the mechanical properties of the whole. It is a significant concept for analyzing the behavior of heterogeneous materials since heterogeneity makes it harder to obtain the mechanical properties of the material. Instead of investigating the whole heterogeneous structure, the smallest volume helps to obtain mechanical properties easier. In a similar way, other material quantities like thermal and optical properties can also be presented by RVE. The main concern of RVE is to represent a macroscopic response by using minimal structure as much as possible [20]. In our study, nano-structures are our interest, and modeling of nano-structures is complex since the dimensions are nanometer and computing power is not enough to analyze nano-scale fiber models. Hence, RVE gains importance in this study.

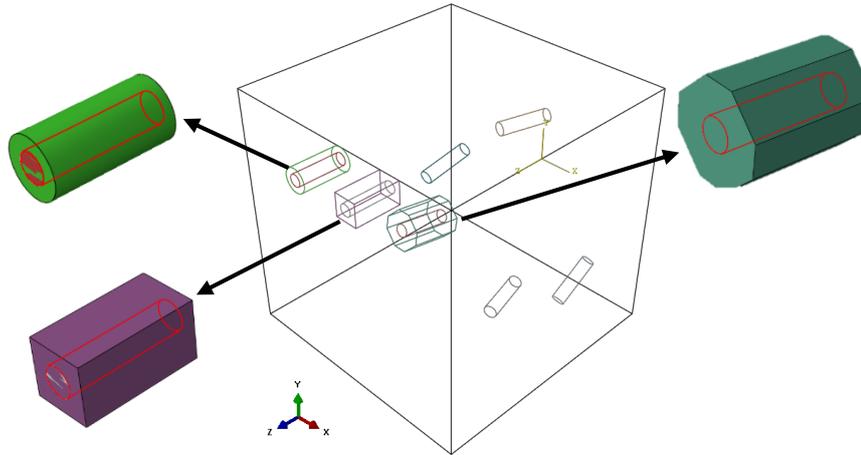


Figure 2.1 Different shapes of RVE

An RVE can be in different shapes such as square, cylindrical, rectangular parallelepiped, or hexagonal, as illustrated in Figure 2.1. Square, cylindrical and rectangular parallelepiped RVEs will be studied in Section 3.1.

One of the criteria for the RVE quality is size determination. As our study is related to CNT-reinforced structures, agglomeration will be a concern for determining RVE size. CNT-reinforced composites are prepared with different manufacturing techniques; however, CNTs agglomerate in the structure due to their chemistry. As a result of agglomeration, clusters occur in the structure. Dispersion problem results in structure properties weakening [21]. Homogeneity generally positively affects the mechanical properties, whereas agglomeration increases the heterogeneity and decreases the strength. Therefore, the volume size can be larger to represent a heterogeneous structure. RVE size can be chosen larger to stay on the conservative side [22].

If fiber materials are uniformly distributed or repeat themselves periodically in a matrix, any RVE taken from the structure will represent the whole structure. If fibers are randomly distributed in the structure, the decision of the RVE size becomes prominent. If the RVE size is chosen close to the size of the whole structure, the

calculation time will take longer. This makes RVE usage meaningless. On the other hand, small RVE can be misleading to compute mechanical properties.

2.2 Embedded Element Method

The Embedded Element Method is a meshing technique in which chosen elements (embedded elements) are embedded in so-called “host” elements. A model with embedded elements can be created by determining the embedded region, the host region, a weight factor, a roundoff tolerance, and an absolute exterior tolerance or fractional exterior tolerance. These properties are used to define geometric tolerance and adjust the position of the nodes. Geometric tolerances are arranged with absolute exterior tolerance or fractional exterior tolerance. The position of the embedded node should be inside of the distance, which is 0.05 times the average size of the non-embedded elements in the model. This tolerance is set by default; however, tolerance can be rearranged by fractional or absolute exterior tolerance values. Fractional exterior tolerance decides that tolerance as a fraction of the average of non-embedded elements. This value is 0.05 by default. On the other hand, absolute exterior tolerance is the absolute value of that distance. If both tolerances are defined, Abaqus picks the smallest value. If a node does not lie in that region, Abaqus gives an error. An embedded node can be relocated in a very small distance when an embedded node is very close to the element edge or element face of the host element. In that cases, that small relocation is performed by weight factor roundoff tolerance [23]. Roundoff tolerance is 10^6 by default. In this study, default values are used.

This meshing technique allows meshing host and embedded elements separately. It means that the host and embedded regions do not have to share the same nodes on the interface between them. Abaqus searches for a geometric relationship between host and embedded region elements node [24]. If nodes of the embedded elements lie in the host region, then these nodes are associated with the nodes of host region elements by shape functions. The host and the embedded regions overlap in this technique, as can be seen in Figure 2.2.

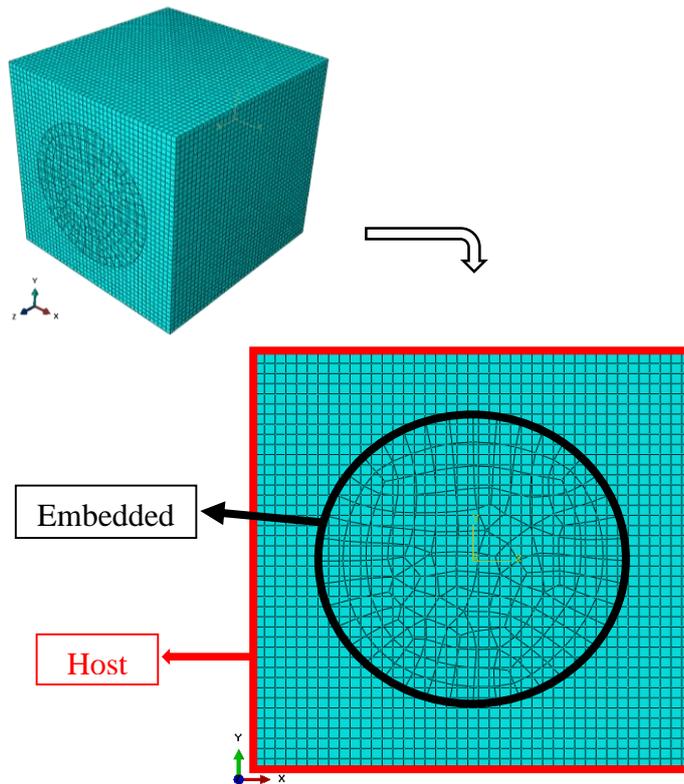


Figure 2.2 Illustration of Embedded and Host Regions

The shape function is a function that interpolates values of a variable at the nodes to points in an element to obtain a solution. It generates an approximation of the field of interest between nodes. Abaqus correlates nodes of embedded elements with shape function. The translational degree of freedom of the embedded element node is ruled out when the node of the embedded element is in the region of host elements. Instead, the translational degree of freedom of the embedded element node is constrained to the interpolated value of the related host element. To present that in Figure 2.3, a node of the embedded element inside the host region is restricted to 4 nodes of the host element, indicated as a dashed arrow mark.

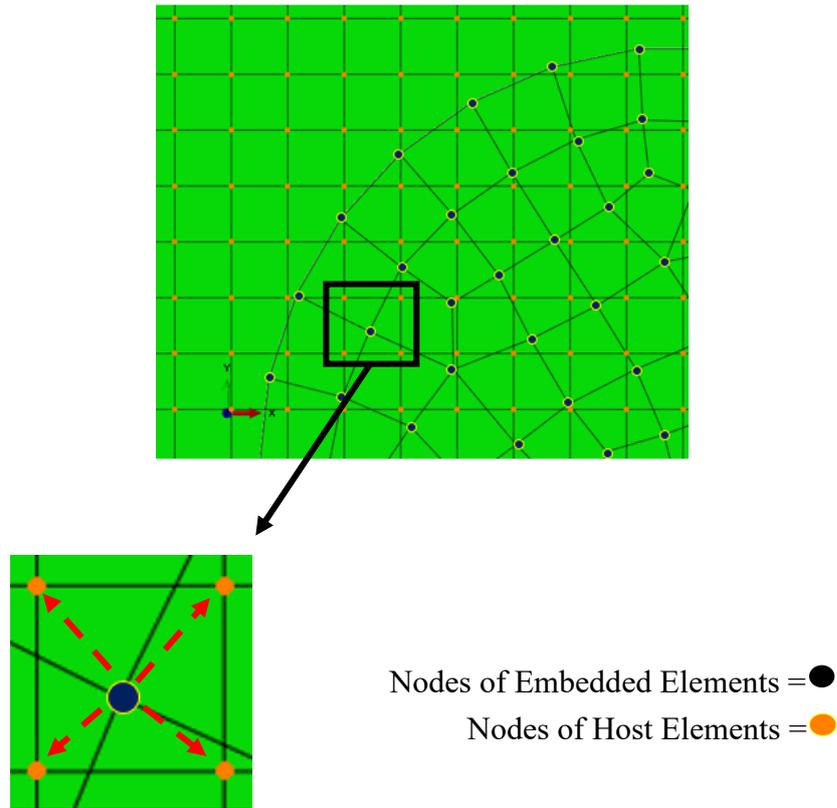


Figure 2.3 Representation of Nodes of Embedded and Host Element

Constraining translational degree of freedom causes Abaqus to include the rigidity of both embedded and host elements. Hence, it gives rise to the whole structure behaving stiffer. Therefore, the elastic modulus of the embedded element should be extracted from the elastic modulus of the host element to prevent not computing the stiffness of both the host and embedded element at the same region. For this reason, a modification is performed for the elastic modulus of fiber as in (2.1).

$$E_{fiber(modified)} = E_{fiber} - E_{matrix} \quad (2.1)$$

2.3 Homogenization Procedure

Heterogeneous materials are comprised of different constituents, and their mechanical properties depend on each constituent. Any sample taken from heterogeneous material can present different mechanical characteristics, unlike homogeneous materials. The homogenization procedure describes the behavior of the heterogeneous material as if it acts as a homogeneous material. Figure 2.4 demonstrates the simple idea of this procedure.

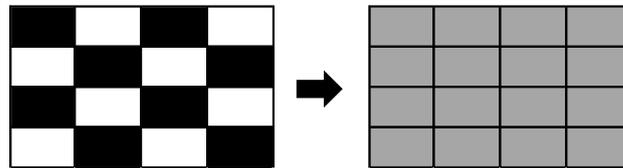


Figure 2.4 Homogenization Procedure

If material is homogeneous, its mechanical properties can be characterized easily on the macroscopic scale. In a heterogeneous case, the macroscopic scale may not be enough to determine these properties. There are several studies to achieve effective elastic modulus of the materials.

Eshelby stated that an isotropic material shows homogeneous deformations if there is no surrounding material around it. The presence of surrounding material causes inclusion to react differently and causes stress inside and outside of the inclusion [25]. Eshelby's tensor gives the relationship between the free strain of the inclusion and matrix strain and is homogeneous in an ellipsoidal inclusion for the classical elasticity problem. There are several approaches to Eshelby's problem. Some of those approaches are the Mori-Tanaka scheme, dilute scheme, Voigt and Reuss bounds. Mori-Tanaka method focuses on the average internal stress in the matrix that contains eigenstrain as a solution to inhomogeneity problems [26]. Its formulation proposes that each inclusion is accepted as single, meaning that they act like they are

isolated in the matrix. It assumes that strain in the matrix shows far-field strain behavior. It can be expressed as [27]:

$$\langle \sigma \rangle = C \langle \varepsilon \rangle \quad (2.2)$$

Benveniste proposed a new approach to the Mori-Tanaka method and described the effective elastic modulus C as [26]:

$$C = (V_m C_m + V_f C_f A) (V_m I + V_f A)^{-1} \quad (2.3)$$

where V_m and V_f are volume fractions of the matrix and the fiber; C_f and C_m are the fourth-order elasticity tensor of the fiber and the matrix, respectively. I is the fourth-order identity tensor. A is the Eshelby strain concentration tensor, and it gives the relationship between the average fiber strain (ε_f) and the matrix strain (ε_m).

$$\varepsilon_f = A \varepsilon_m \quad (2.4)$$

$$A = [I + S(C_m)^{-1} (C_f - C_m)]^{-1} \quad (2.5)$$

Eshelby tensor is denoted as S in (2.5).

The dilute scheme proposes that each inhomogeneity is independent and isolated in the media. It assumes that inclusions do not interact with each other. Homogenized elasticity tensor is given as below [28]:

$$C_{dilute} = C_m + \sum_{i=2}^{i=N} V_i (C_i - C_m) : A_i \quad (2.6)$$

C_{dilute} , C_m , C_i , V_i and A_i are the dilute scheme elasticity tensor, elasticity tensor of matrix, elasticity tensor of inclusion i , volume fraction of inclusion i and concentration tensor of inclusion i .

Other approaches are Voigt and Reuss Bounds. Voigt bound assumes that the strain is constant all over the media. In other words, Voigt bound is an isostrain model which is springs in parallel. On the other hand, Reuss bound states that the stress is constant in the media, and stress summation is the same as the stress in the macroscopic state. This approach is an isostress model, and it behaves like springs

in series [29]. Voigt and Reuss bound can be expressed as in (2.7) and (2.8), respectively [28]:

$$\mathbf{C}^{voigt} = \sum_{i=1}^{i=N} V_i \mathbf{C}_i \quad (2.7)$$

$$\mathbf{S}^{reuss} = \sum_{i=1}^{i=N} V_i \mathbf{C}_i^{-1} \quad (2.8)$$

where \mathbf{C}^{voigt} and \mathbf{S}^{reuss} represents the Voigt and the Reuss elasticity tensors, respectively. V_i stands for the volume fraction of the inclusions, and \mathbf{C}_i is the elasticity tensor of the related component.

The voigt bound corresponds to the upper bound of the effective elastic modulus of the composite. It is the maximum stiffness limit of the structure that it can have. Also, the Reuss bound is the lower bound of the structure. It implies that the stiffness of the composite cannot be lower than the Reuss bound.

There are other approaches to finding a solution for the heterogeneity problem; some are explained above to give the main idea. All of the expressed approaches have the same objective: to observe the effective elastic modulus of the heterogeneous medium.

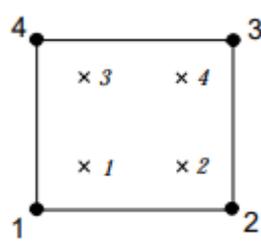
2.3.1 Averaging

Homogenization is an approach to compute the effective properties of heterogeneous materials. If properly used, the averaging method facilitates calculations in the homogenization process.

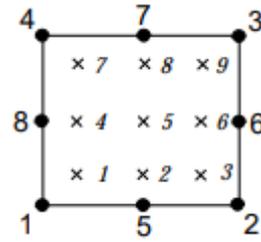
Each element in the model has its stress and strain value at its integration point. In order to operate on these quantities, it is necessary to understand how the software works. In this study, Abaqus is chosen as FEM software. Abaqus utilizes the volume of each element to integrate different quantities, and material response in each element is calculated at the integration points. There are two integration alternatives for the analysis, full or reduced integration. The main difference between these

integrations is the number of integration points used for the stiffness matrix formulation. The integration points represent Gauss points, and Gauss points determine the accuracy of the calculations. Full integration means that the stiffness matrix is computed in each Gauss point. On the other hand, reduced integration removes high-order terms of the formula to simplify calculations and uses fewer Gauss points.

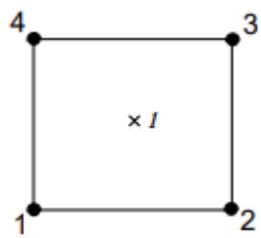
Figure 2.5 demonstrates the integration points for the full integration and reduced integration models.



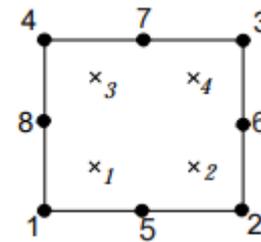
(a) Linear element



(b) Quadratic element



(c) Linear element



(d) Quadratic element

Figure 2.5 Integrations points (a)(b) for fully integrated elements, (c)(d) with reduced integration elements [23]

Figure 2.5 (a) shows two integration points in each direction for fully integrated linear elements. On the other hand, the reduced integration model has a single integration point at the center (Figure 2.5 (c)).

For quadrilateral elements, full integration has three integration points in each direction (Figure 2.5(b)). These integration points decrease to two in each direction with the reduced integration (Figure 2.5(d)).

Choose of full integration or reduced integration affects the accuracy of the analysis. Full integration gives better results since all Gauss points are included in the calculation. However, the cost of computation time should be considered. Conversely, reduced integration provides less computational time due to decreased number of integration points. In general, the stiffness matrix is overestimated based on displacement-based finite element formulations. Fewer integration points can be preferred in order to model less stiff elements in some cases, like non-linear plasticity problems. According to the requirements, model selection depends on the user's action. In this study, three-dimensional full integration elements will be used as accuracy is one of the primary considerations. Also, the interest of study does not cover the plastic behavior of the heterogeneous structure.

Each element in the model has its stress and strain value at its integration point. The effect of each element is different, and to consider this influence, weight function will be used in this regard. Weight function allows the more weighted element to affect the results more than less weighted elements. Integration point volume (IVOL) value is taken into consideration for weight function and homogenization procedure. Average stress and strain values will be achieved with weight function so that these values will be used in the stiffness matrix. It means that total macroscopic stress and strain values will be the average of the local stresses and strains in a given volume. Total stress (ε_{total}) and strain (σ_{total}) values in a described volume Ω can be written as in (2.9) and (2.10) [30].

$$\varepsilon_{total} = \int_{\Omega} \varepsilon(x) d\Omega \quad (2.9)$$

$$\sigma_{total} = \int_{\Omega} \sigma(x) d\Omega \quad (2.10)$$

Average stress ($\sigma_{average}$) and strain ($\epsilon_{average}$) values can be written as:

$$\epsilon_{average} = \frac{1}{|\Omega|} \int_{\Omega} \epsilon(x) d\Omega \quad (2.11)$$

$$\sigma_{average} = \frac{1}{|\Omega|} \int_{\Omega} \sigma(x) d\Omega \quad (2.12)$$

In our model, averaging is implemented by utilizing the weight function to achieve more satisfactory results for homogenization. Hence, stress and strain tensors at each integration point are multiplied with corresponding volumes of the integration points (IVOL values). According to the finite element model, averaging with weight function is shown in Equation (2.13) and Equation (2.14) :

$$\bar{\sigma} = \frac{\sum_{i=1}^n \sigma_i V_i}{\sum_{i=1}^n V_i} \quad (2.13)$$

$$\bar{\epsilon} = \frac{\sum_{i=1}^n \epsilon_i V_i}{\sum_{i=1}^n V_i} \quad (2.14)$$

Where,

$\bar{\sigma}$: Homogenized stress tensor

$\bar{\epsilon}$: Homogenized strain tensor

σ_i : Stress at integration point i

ϵ_i : Strain at integration point i

V_i : Volume of integration point i

n : Total number of integration points

Abaqus stores IVOL values, stress, and strain values for every integration point. Appendix A includes averaging calculations with Python code.

2.3.2 Stiffness and Compliance Matrices

The stiffness tensor \mathbf{C} is used to express the stress-strain relation of materials. In the most general case of anisotropic linear elasticity, it has 81 components [31].

$$\begin{bmatrix} \sigma_{11} \\ \sigma_{12} \\ \sigma_{13} \\ \sigma_{21} \\ \sigma_{22} \\ \sigma_{23} \\ \sigma_{31} \\ \sigma_{32} \\ \sigma_{33} \end{bmatrix} = \begin{bmatrix} C_{1111} & C_{1112} & C_{1113} & C_{1121} & C_{1122} & C_{1123} & C_{1131} & C_{1132} & C_{1133} \\ C_{1211} & C_{1212} & C_{1213} & C_{1221} & C_{1222} & C_{1223} & C_{1231} & C_{1232} & C_{1233} \\ C_{1311} & C_{1312} & C_{1313} & C_{1321} & C_{1322} & C_{1323} & C_{1331} & C_{1332} & C_{1333} \\ C_{2111} & C_{2112} & C_{2113} & C_{2121} & C_{2122} & C_{2123} & C_{2131} & C_{2132} & C_{2133} \\ C_{2211} & C_{2212} & C_{2213} & C_{2221} & C_{2222} & C_{2223} & C_{2231} & C_{2232} & C_{2233} \\ C_{2311} & C_{2312} & C_{2313} & C_{2321} & C_{2322} & C_{2323} & C_{2331} & C_{2332} & C_{2333} \\ C_{3111} & C_{3112} & C_{3113} & C_{3121} & C_{3122} & C_{3123} & C_{3131} & C_{3132} & C_{3133} \\ C_{3211} & C_{3212} & C_{3213} & C_{3221} & C_{3222} & C_{3223} & C_{3231} & C_{3232} & C_{3233} \\ C_{3311} & C_{3312} & C_{3313} & C_{3321} & C_{3322} & C_{3323} & C_{3331} & C_{3332} & C_{3333} \end{bmatrix} \cdot \begin{bmatrix} \varepsilon_{11} \\ \varepsilon_{12} \\ \varepsilon_{13} \\ \varepsilon_{21} \\ \varepsilon_{22} \\ \varepsilon_{23} \\ \varepsilon_{31} \\ \varepsilon_{32} \\ \varepsilon_{33} \end{bmatrix} \quad (2.15)$$

The 4th order stiffness tensor C_{ijkl} shows minor symmetry. If it provides the condition below [32]:

$$C_{ijkl} = C_{jikl} \quad \& \quad C_{ijkl} = C_{ijlk} \quad (2.16)$$

The first and second equalities are called left and right minor symmetry, respectively. Tensor has 36 independent components if minor symmetry exists.

For major symmetry, tensor also satisfies the following condition:

$$C_{ijkl} = C_{klij} \quad (2.17)$$

With this condition, tensor has 21 independent components.

Equation (2.15) is simplified to (2.18) by using major and minor symmetry conditions [33].

$$\begin{bmatrix} \sigma_{11} \\ \sigma_{22} \\ \sigma_{33} \\ \sigma_{23} \\ \sigma_{13} \\ \sigma_{12} \end{bmatrix} = \begin{bmatrix} C_{1111} & C_{1122} & C_{1133} & C_{1123} & C_{1113} & C_{1112} \\ & C_{2222} & C_{2233} & C_{2223} & C_{2213} & C_{2212} \\ & & C_{3333} & C_{3323} & C_{3313} & C_{3312} \\ & & & C_{2323} & C_{2313} & C_{2312} \\ & & & & C_{1313} & C_{1312} \\ & & & & & C_{1212} \end{bmatrix} \begin{bmatrix} \varepsilon_{11} \\ \varepsilon_{22} \\ \varepsilon_{33} \\ 2 \varepsilon_{23} \\ 2 \varepsilon_{13} \\ 2 \varepsilon_{12} \end{bmatrix} \quad (2.18)$$

Symmetric

There are symmetric components in (2.18) ($\varepsilon_{23} = \varepsilon_{32}$, $\varepsilon_{13} = \varepsilon_{31}$, $\varepsilon_{12} = \varepsilon_{21}$). Engineering shear strains can be written as sum of symmetric components to simplify matrix ($2 \varepsilon_{23} = \varepsilon_4$, $2 \varepsilon_{13} = \varepsilon_5$, $2 \varepsilon_{12} = \varepsilon_6$). The equation becomes (2.19):

$$\begin{bmatrix} \sigma_1 \\ \sigma_2 \\ \sigma_3 \\ \sigma_4 \\ \sigma_5 \\ \sigma_6 \end{bmatrix} = \begin{bmatrix} C_{11} & C_{12} & C_{13} & C_{14} & C_{15} & C_{16} \\ & C_{22} & C_{23} & C_{24} & C_{25} & C_{26} \\ & & C_{33} & C_{34} & C_{35} & C_{36} \\ & & & C_{44} & C_{45} & C_{46} \\ & & & & C_{55} & C_{56} \\ & & & & & C_{66} \end{bmatrix} \begin{bmatrix} \varepsilon_1 \\ \varepsilon_2 \\ \varepsilon_3 \\ \varepsilon_4 \\ \varepsilon_5 \\ \varepsilon_6 \end{bmatrix} \quad (2.19)$$

The stress-strain relation in (2.19) can be written as six linear scalar equations.

$$\begin{aligned} \sigma_1 &= C_{11} \varepsilon_1 + C_{12} \varepsilon_2 + C_{13} \varepsilon_3 + C_{14} \varepsilon_4 + C_{15} \varepsilon_5 + C_{16} \varepsilon_6 \\ \sigma_2 &= C_{21} \varepsilon_1 + C_{22} \varepsilon_2 + C_{23} \varepsilon_3 + C_{24} \varepsilon_4 + C_{25} \varepsilon_5 + C_{26} \varepsilon_6 \\ \sigma_3 &= C_{31} \varepsilon_1 + C_{32} \varepsilon_2 + C_{33} \varepsilon_3 + C_{34} \varepsilon_4 + C_{35} \varepsilon_5 + C_{36} \varepsilon_6 \\ \sigma_4 &= C_{41} \varepsilon_1 + C_{42} \varepsilon_2 + C_{43} \varepsilon_3 + C_{44} \varepsilon_4 + C_{45} \varepsilon_5 + C_{46} \varepsilon_6 \\ \sigma_5 &= C_{51} \varepsilon_1 + C_{52} \varepsilon_2 + C_{53} \varepsilon_3 + C_{54} \varepsilon_4 + C_{55} \varepsilon_5 + C_{56} \varepsilon_6 \\ \sigma_6 &= C_{61} \varepsilon_1 + C_{62} \varepsilon_2 + C_{63} \varepsilon_3 + C_{64} \varepsilon_4 + C_{65} \varepsilon_5 + C_{66} \varepsilon_6 \end{aligned} \quad (2.20)$$

The stress and strain values are necessary to obtain components of the elasticity tensor. For this reason, a macroscopic strain is applied to the model and the homogenized stress components are computed with the finite element software Abaqus.

As stated before, a composite reinforced with a single straight CNT demonstrates orthotropic behavior. For orthotropic materials, (2.19) is further simplified:

$$\begin{bmatrix} \sigma_1 \\ \sigma_2 \\ \sigma_3 \\ \sigma_4 \\ \sigma_5 \\ \sigma_6 \end{bmatrix} = \begin{bmatrix} C_{11} & C_{12} & C_{13} & 0 & 0 & 0 \\ & C_{22} & C_{23} & 0 & 0 & 0 \\ & & C_{33} & 0 & 0 & 0 \\ & & & C_{44} & 0 & 0 \\ & & & & C_{55} & 0 \\ & & & & & C_{66} \end{bmatrix} \begin{bmatrix} \varepsilon_1 \\ \varepsilon_2 \\ \varepsilon_3 \\ \varepsilon_4 \\ \varepsilon_5 \\ \varepsilon_6 \end{bmatrix} \quad (2.21)$$

Six different macroscopic strains are separately applied to the RVE to determine the components of the homogenized elasticity matrix. The first three columns of the matrix (C_{11} , C_{12} , C_{13} , C_{22} , C_{23} , C_{33}) are obtained from three different uniaxial tensile tests, while the rest (C_{44} , C_{55} , C_{66}) are obtained from three different shear deformations.

For example, in the first uniaxial deformation case $\varepsilon_1 \neq 0$, and the other macroscopic strains are set to 0 ($\varepsilon_2 = \varepsilon_3 = \varepsilon_4 = \varepsilon_5 = \varepsilon_6 = 0$) to find C_{11} component of the matrix (see (2.22)).

$$\sigma_1 = C_{11} \cdot \varepsilon_1 + \underbrace{C_{12} \cdot \varepsilon_2}_{0} + \underbrace{C_{13} \cdot \varepsilon_3}_{0} + \underbrace{C_{14} \cdot \varepsilon_4}_{0} + \underbrace{C_{15} \cdot \varepsilon_5}_{0} + \underbrace{C_{16} \cdot \varepsilon_6}_{0} \quad (2.22)$$

$$\sigma_1 = C_{11} \cdot \varepsilon_1$$

The same procedure is applied to obtain other components of the matrix. C_{12} and C_{13} are determined using the second and the third equations in (2.20) for the same uniaxial loading case. From the other uniaxial load cases, C_{22} , C_{23} and C_{33} are obtained similarly. Finally, C_{44} , C_{55} and C_{66} are computed from the three shear deformations.

After finding the components of the elasticity matrix, the compliance matrix could also be computed. The relationship between the compliance and elasticity matrices is as below.

$$\mathbf{C}^{-1} = \mathbf{S} \quad (2.23)$$

The stress-strain relation for isotropic linear elastic material reads:

$$\begin{bmatrix} \sigma_1 \\ \sigma_2 \\ \sigma_3 \\ \sigma_4 \\ \sigma_5 \\ \sigma_6 \end{bmatrix} = \xi \begin{bmatrix} 1-\nu & \nu & \nu & 0 & 0 & 0 \\ \nu & 1-\nu & \nu & 0 & 0 & 0 \\ \nu & \nu & 1-\nu & 0 & 0 & 0 \\ 0 & 0 & 0 & 1-2\nu & 0 & 0 \\ 0 & 0 & 0 & 0 & 1-2\nu & 0 \\ 0 & 0 & 0 & 0 & 0 & 1-2\nu \end{bmatrix} \begin{bmatrix} \varepsilon_1 \\ \varepsilon_2 \\ \varepsilon_3 \\ \varepsilon_4 \\ \varepsilon_5 \\ \varepsilon_6 \end{bmatrix} \quad (2.24)$$

where ξ is :

$$\xi = \frac{E}{(1+\nu)(1-2\nu)} \quad (2.25)$$

Similarly, an inverse relation can be written as:

$$\begin{bmatrix} \varepsilon_1 \\ \varepsilon_2 \\ \varepsilon_3 \\ \varepsilon_4 \\ \varepsilon_5 \\ \varepsilon_6 \end{bmatrix} = \frac{1}{E} \begin{bmatrix} 1 & -\nu & -\nu & 0 & 0 & 0 \\ -\nu & 1 & -\nu & 0 & 0 & 0 \\ -\nu & -\nu & 1 & 0 & 0 & 0 \\ 0 & 0 & 0 & 1+\nu & 0 & 0 \\ 0 & 0 & 0 & 0 & 1+\nu & 0 \\ 0 & 0 & 0 & 0 & 0 & 1+\nu \end{bmatrix} \begin{bmatrix} \sigma_1 \\ \sigma_2 \\ \sigma_3 \\ \sigma_4 \\ \sigma_5 \\ \sigma_6 \end{bmatrix} \quad (2.26)$$

These relations are true for isotropic materials. For orthotropic materials, components will be different. Orthotropic material behavior should be comprehended at first to convert these relations. There are two mutually orthogonal directions for orthotropic materials. Orthotropy causes that tension load produces only parallel and perpendicular stress according to load implementation direction, and shear load creates shear strain only. This provides equation below [34]:

$$\sigma_i = Q_{ij} \varepsilon_j \quad (2.27)$$

Where Q_{ij} is stiffness matrix and $i, j = 1, 2, 3, 4, 5, 6$. According to these conditions, stiffness matrix for orthotropic materials become as (2.28):

$$\begin{bmatrix} \sigma_{11} \\ \sigma_{22} \\ \sigma_{33} \\ \sigma_{23} \\ \sigma_{13} \\ \sigma_{12} \end{bmatrix} = \begin{bmatrix} Q_{11} & Q_{12} & Q_{13} & 0 & 0 & 0 \\ & Q_{22} & Q_{23} & 0 & 0 & 0 \\ & & Q_{33} & 0 & 0 & 0 \\ & & & Q_{44} & 0 & 0 \\ & & & & Q_{55} & 0 \\ & & & & & Q_{66} \end{bmatrix} \begin{bmatrix} \varepsilon_{11} \\ \varepsilon_{22} \\ \varepsilon_{33} \\ \varepsilon_{23} \\ \varepsilon_{13} \\ \varepsilon_{12} \end{bmatrix} \quad (2.28)$$

Equation (2.28) has 9 elastic constants to express orthotropic material.

For plane stress condition, out of plane stresses will be zero ($\sigma_3 = \sigma_{23} = \sigma_{31} = 0$).

If plane stress condition is applied to (2.28), Equation (2.29) is achieved and the reduced stiffness matrix can be written as (2.30).

$$\begin{bmatrix} \sigma_{11} \\ \sigma_{22} \\ 0 \\ 0 \\ 0 \\ \sigma_{12} \end{bmatrix} = \begin{bmatrix} Q_{11} & Q_{12} & Q_{13} & 0 & 0 & 0 \\ & Q_{22} & Q_{23} & 0 & 0 & 0 \\ & & Q_{33} & 0 & 0 & 0 \\ & & & Q_{44} & 0 & 0 \\ & & & & Q_{55} & 0 \\ & & & & & Q_{66} \end{bmatrix} \begin{bmatrix} \varepsilon_{11} \\ \varepsilon_{22} \\ \varepsilon_{33} \\ \varepsilon_{23} \\ \varepsilon_{13} \\ \varepsilon_{12} \end{bmatrix} \quad (2.29)$$

$$\begin{bmatrix} \sigma_{11} \\ \sigma_{22} \\ \sigma_{12} \end{bmatrix} = \begin{bmatrix} Q_{11} & Q_{12} & 0 \\ Q_{12} & Q_{22} & 0 \\ 0 & 0 & Q_{66} \end{bmatrix} \begin{bmatrix} \varepsilon_{11} \\ \varepsilon_{22} \\ \varepsilon_{12} \end{bmatrix} \quad (2.30)$$

As a result, Equation (2.30) leads us to describe the compliance matrix as below:

$$\begin{bmatrix} \varepsilon_{11} \\ \varepsilon_{22} \\ \varepsilon_{12} \end{bmatrix} = \begin{bmatrix} S_{11} & S_{12} & 0 \\ S_{12} & S_{22} & 0 \\ 0 & 0 & S_{66} \end{bmatrix} \begin{bmatrix} \sigma_{11} \\ \sigma_{22} \\ \sigma_{12} \end{bmatrix} \quad (2.31)$$

By using relation between the compliance and the stiffness matrix, elastic modulus, shear modulus and Poisson ratio values are as follows respectively in (2.32), (2.33), (2.34) :

$$E_{11} = \frac{1}{S_{11}} \quad E_{22} = \frac{1}{S_{22}} \quad E_{33} = \frac{1}{S_{33}} \quad (2.32)$$

$$G_{23} = \frac{1}{2 S_{44}} \quad G_{31} = \frac{1}{2 S_{55}} \quad G_{12} = \frac{1}{2 S_{66}} \quad (2.33)$$

$$v_{23} = -S_{32} E_{22} \quad v_{31} = -S_{13} E_{33} \quad v_{12} = -S_{21} E_{11} \quad (2.34)$$

$$v_{32} = -S_{23} E_{33} \quad v_{13} = -S_{31} E_{11} \quad v_{21} = -S_{12} E_{22}$$

Abaqus Scripting Interface allows Python 2.7 to interact with stored data in Abaqus. Therefore, a Python script is used to modify results coming from Abaqus analysis. Appendix A includes the related Python script to find elasticity and compliance matrices.

2.3.3 Boundary Conditions

In this study, six different load cases are considered separately to solve the problem. These are three uniaxial tensile displacements ($\varepsilon_1, \varepsilon_2, \varepsilon_3$) and three shear deformations ($\varepsilon_4, \varepsilon_5, \varepsilon_6$). One of the macroscopic strain components is set to a non-zero value in each load case. The rest of the macroscopic strain components are set to zero (check Equation (2.22)). This procedure is repeated for each load case. The boundary conditions applied correspond to uniform displacement boundary conditions and present the upper bound in homogenization theory.

For example, when $\varepsilon_1 \neq 0$, the rest of the strain components are set to zero ($\varepsilon_2 = \varepsilon_3 = \varepsilon_4 = \varepsilon_5 = \varepsilon_6 = 0$). The boundary conditions of the six different load cases are demonstrated in Figure 2.6.

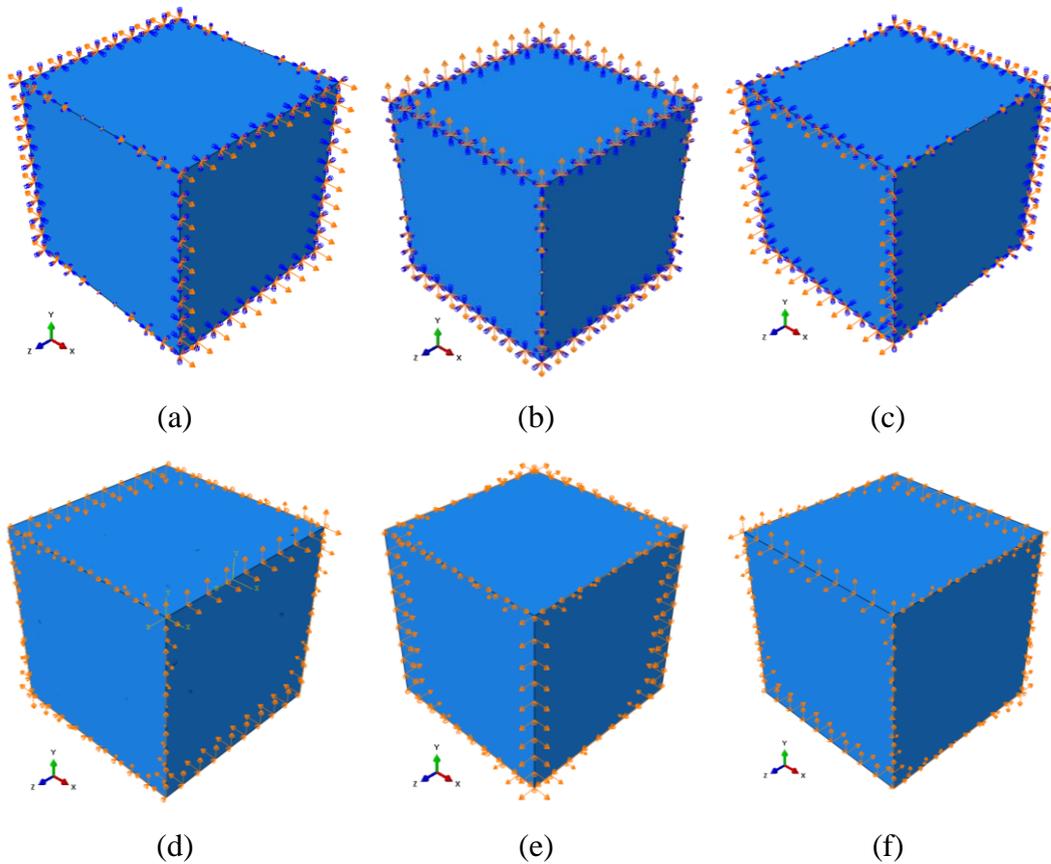


Figure 2.6 Representation of boundary conditions for three tensile a) ε_1 , b) ε_2 , c) ε_3 , and three shear d) ε_4 , e) ε_5 , f) ε_6 load cases

2.4 Random Sequential Adsorption Algorithm

Heterogeneous materials keep different materials inside them by definition, and one of the reasons that cause the structure to be heterogeneous is randomness. In this study, CNT reinforced composites are our interest, and CNT material exists randomly in the matrix. There are several approaches to model random dispersion. Those methods are basic Random Sequential Adsorption (RSA), modified Random Sequential Adsorption (RSA), Monte Carlo, collective rearrangement, and random walk.

Random Sequential Adsorption (RSA) algorithm is a method to place particles in a specified place randomly. In this method, particles do not overlap or intersect with each other. Since it is a sequential process, when a particle is placed in a system, its position is fixed. The method tries to find a suitable place for the next particle. It is the basic RSA definition. In the modified RSA method, specified regions can be divided into different pieces such as layers, cubes, or other shapes.

The Monte Carlo method is a probabilistic approach to random modeling. It creates random numbers in the given range and uses a probability distribution function. Firstly, it arranges the fiber placement and orientations, and then reduces the volume of the initial space to reach the desired volume fraction.

The collective rearrangement method uses sphere particle shapes. It decides which spheres to be picked randomly. In this method, domain size, type, and size of particles should be defined at first. According to the volume fraction, the number of particles is decided and placed randomly. This method can be used for nonspherical models when modified [35].

The random walk is a stochastic process that a point follows different probable paths. Origin is decided at the beginning, and all possible ways are determined for that position. According to the random pick, the point moves to the next spot. Some modifications should be made to implement this method to random fiber placement since the history does not affect the future move. It means that the point can go back to the previous location, and this causes overlapping or intersection.

The maximum volume fraction (V_f) and aspect ratio (AR) of the fibers have some restrictions according to which method is applied. A comparison of these methods is represented in Table 2.1 [36].

Table 2.1 Random fiber generation methods, their related volume fractions and aspect ratios

Method	V_f (max)[%]	AR (max)	Reference
Basic RSA	15	5	[37]
Modified RSA (jamming limit)	40	Varies	[30]
Modified RSA (fixed aspect ratio fibers)	55	10	[38]
Modified RSA (sublayers-2D)	35	20	[39]
Monte Carlo	20	10	[40]
Collective Rearrangement	35	10	[41]
Random walk	70	9	[42]

In this study, the RSA algorithm is used. Its volume fraction value is enough for CNT-reinforced composites. Also, this method can be applied by dividing RVE into small pieces, which ease the modeling. The RSA algorithm needs the parts not to clash with each other. Once a particle is located, its location is no longer available for the other particles. The placement of the particles can be created with different approaches.

One of these approaches is to create a point and corresponding vector. Zhou et al. [43] studied the RSA algorithm to place fibers into a matrix. According to this, firstly, a point in the given region is created randomly. After that, a random unit vector is formed. According to fiber length and unit vector, the second point is created. These points generate the first fiber. Then the same procedure is repeated to create the second fiber. To prevent the intersection of these fibers, the minimum distance between points should be greater than the diameter of the fiber. The created two vectors are shown in Figure 2.7. If this condition holds, the program continues to check each point generated. The limit for this random generation is the volume

fraction which is about 15%. This upper limit is more than enough for CNT-reinforced nanocomposites. Their process diagram can be seen in Figure 2.8.

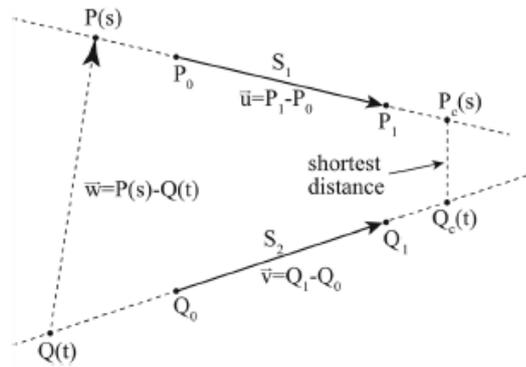


Figure 2.7 Main idea of the creating and placing fibers according to Modified RSA Algorithm [43]

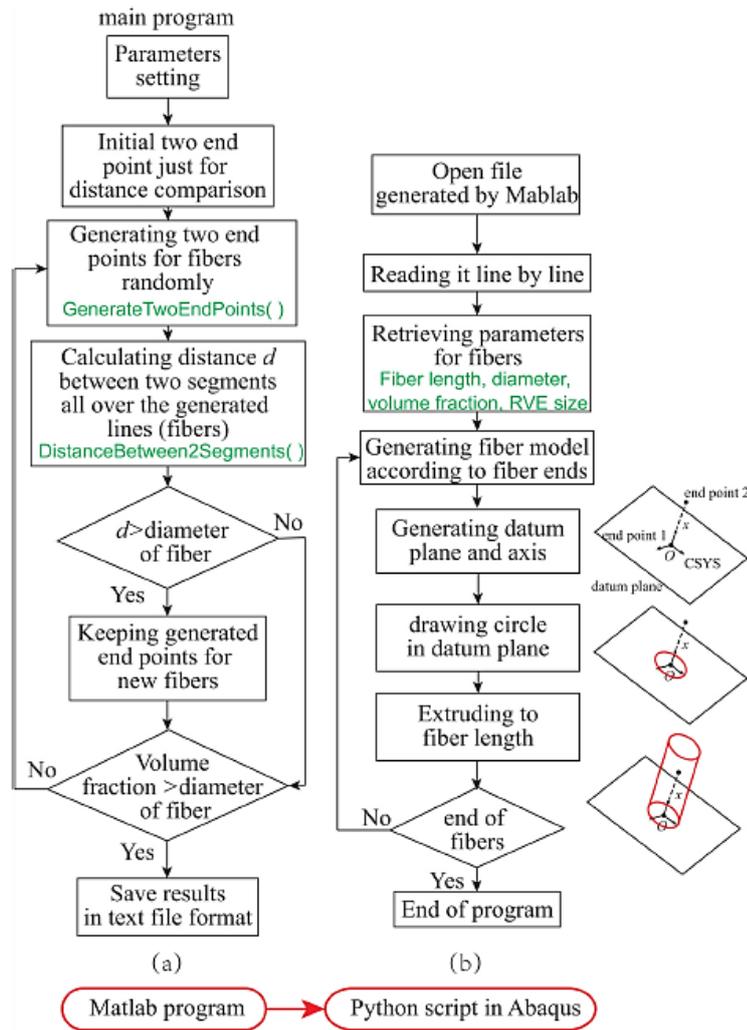


Figure 2.8 Modified RSA Algorithm Flow Chart [43]

Another way to create random fibers with the RSA algorithm is to divide given volume into small pieces. The shape of the divided parts can change according to the requirement and the problem. It can be a sphere, layer, cube, or any customized shape. In this study, the cube is chosen as a sub-volume. The size of smaller cubes is decided according to the fiber dimension. The particles do not overlap as they are placed into sub-volume.

2.5 Rule of Mixtures

The rule of mixtures is an approximation method for composite material elastic properties using the volume-weighted average of the components. However, this method computes elastic properties suggesting that the process is linear and the materials are homogeneous. Hence, the rule of mixture results tends to overestimate. Even though it overestimates, the rule of mixtures provides general insight into the new composite properties. In general form, the rule of mixtures can be described as follows:

$$\Psi = \left[\xi (\Psi^{(i)})^\beta + (1 - \xi)(\Psi^{(m)})^\beta \right]^{\frac{1}{\beta}} \quad (2.35)$$

where Ψ is the scalar property of two-phase composite, ξ is the volume fraction of the phases, superscripts i and m describe the composite components, and β is an exponent to be picked to get relevant results for the test data [29].

In this equation, $\beta = 1$ and $\beta = -1$ stand for the upper and the lower bound, respectively. The upper and the lower bound are also known as Voigt and Reuss bound. Voigt bound describes the isostrain model. On the other hand, Reuss bound corresponds to the isostress model. Figure 2.9 shows Voigt and Reuss models.

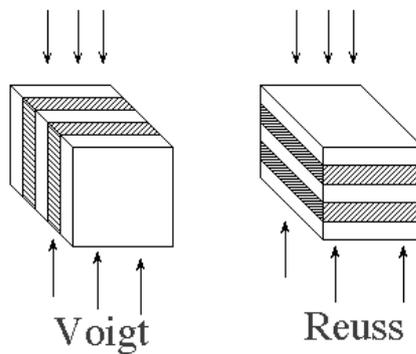


Figure 2.9 Voigt and Reuss model representation [44]

According to these explanations, Voigt (2.36) and Reuss bound (2.37) for the Young's modulus can be described as follows:

$$E_{c, longitudinal} = E_m \cdot V_m + E_f \cdot V_f \quad (2.36)$$

$$\frac{1}{E_{c, transverse}} = \frac{V_m}{E_m} + \frac{V_f}{E_f} \quad (2.37)$$

Where,

E_m : Elastic modulus of matrix

E_f : Elastic modulus of fiber

V_m : Volume fraction of matrix

V_f : Volume fraction of fiber

$E_{c, longitudinal}$: Longitudinal elastic modulus of composite

$E_{c, transverse}$: Transverse elastic modulus of composite

Results from the rule of mixtures will be used to comprehend the difference between the rule of mixtures and the homogenization solution. The upper and the lower bounds are determiners to examine whether the results are in a suitable range or not.

CHAPTER 3

VALIDATION STUDIES

In this chapter, validation studies are explained. Firstly, RVE is the starting point for the study. For this reason, the effects of RVE shapes are investigated. Mesh convergence study is presented. The results of RVEs with embedded and partitioned CNTs are compared. CNT placement (embedded in the matrix or throughout matrix) in RVE is checked. After those studies, one of the articles is reanalyzed. The Voigt and the Reuss bound are also considered.

3.1 Mesh Convergence Study

Mesh quality is one of the considerations for validation. Mesh size should be decided before comparing embedded and partitioned models. Therefore, three different mesh sizes, i.e., coarse, normal, and fine, are considered. Table 3.1 and Figure 3.1 show mesh quality parameters and models, respectively. Dimension and property of the model can be found in Table 3.5 and Table 3.6, respectively. The rectangular model is studied for the mesh quality study. The element size for coarse, normal, and fine mesh is chosen as 10%, 5%, and 2% of the edge length, respectively.

Table 3.1 Mesh quality parameters

	Coarse	Normal	Fine
Approximate element size [nm]	8	4	2
Total number of nodes	3080	16848	123012
Total number of elements	2561	15075	116150

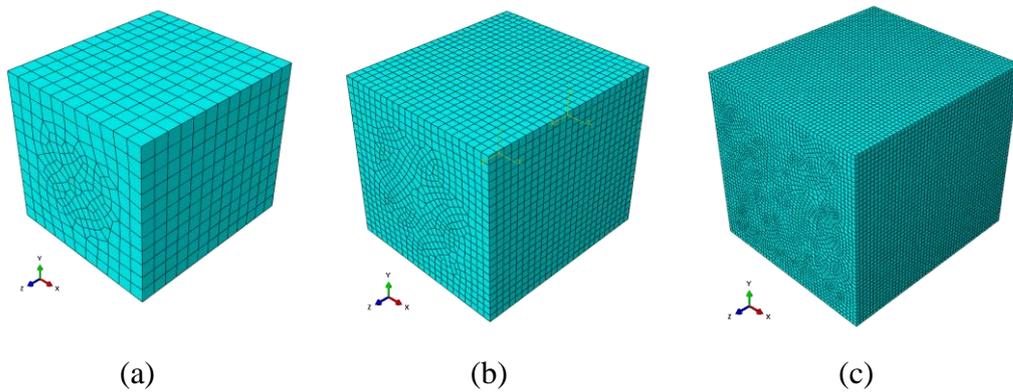


Figure 3.1 Models for (a) coarse, (b) normal and (c) fine meshes

Table 3.2 Elastic modulus results of mesh quality study

	E₁ [MPa]	E₂ [MPa]	E₃ [MPa]
Coarse	4221.7	4224.9	12583.5
Normal	4256.4	4356.4	13315.5
Fine	4378.0	4377.6	13321.3

Table 3.3 Shear modulus results of mesh quality study

	G₁₂ [MPa]	G₁₃ [MPa]	G₂₃ [MPa]
Coarse	740.5	735.5	735.5
Normal	750.3	750.6	750.7
Fine	748.8	750.7	750.7

Table 3.4 Poisson's Ratio results of mesh quality study

	v₁₂ [-]	v₁₃ [-]	v₂₃ [-]
Coarse	0.47	0.35	0.35
Normal	0.47	0.36	0.34
Fine	0.46	0.35	0.35

In Table 3.2, Table 3.3, and Table 3.4, homogenized elastic constants for three different mesh sizes are presented.

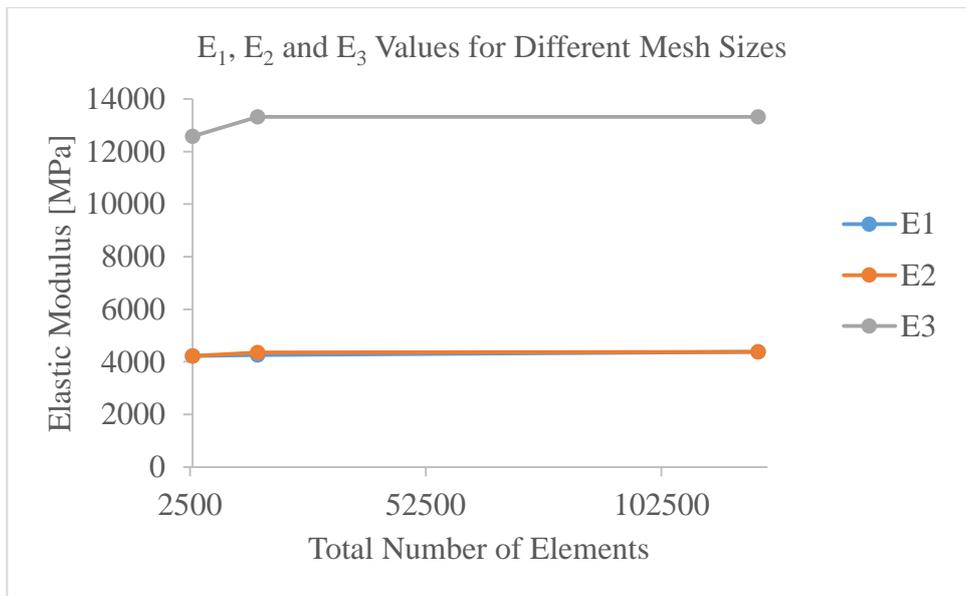


Figure 3.2 E₁, E₂, and E₃ values for different mesh sizes (from coarse to fine)

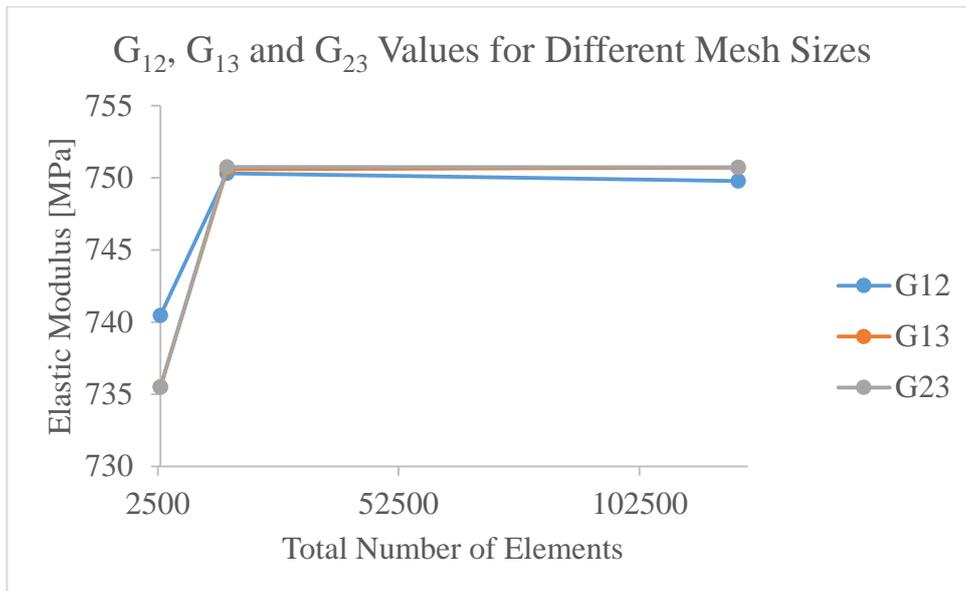


Figure 3.3 G₁₂, G₁₃, and G₂₃ values for different mesh sizes (from coarse to fine)

As can be seen in Figure 3.2 and Figure 3.3, results converge with the decrease in element size. However, the normal mesh results are very close to fine mesh results..

Therefore, the normal mesh size is chosen considering the desired accuracy and the computational cost.

3.2 Effects of RVE Shapes

RVE shape should be considered since the study starts with RVE. Different shapes of RVE are considered in this section to understand whether the RVE shape affects the results. Rectangular, cylindrical, and hexagonal shapes are chosen. Volume fraction, which is 1%, and CNT dimension are kept the same for all samples to understand the effect of the RVE shape. Dimensions and mechanical properties can be found in Table 3.5 and Table 3.6, respectively. The length of the RVE is the same as the length of the CNT in all models. Sample models can be seen in Figure 3.4.

Table 3.5 Dimension of samples [nm]

D_{CNT}	L_{CNT}	D_{cylindrical}	L_{rectangular}	L_{hexagonal}
10	100	100	88.62	54.98

Table 3.6 Mechanical properties of fiber and matrix

	Elastic Modulus [GPa]	Poisson's Ratio [-]
CNT	1000	0.25
Matrix	3.7	0.35

Mechanical properties of CNT and matrix, i.e., PEEK, material are decided according to previous researches and supplier data [45]-[46].

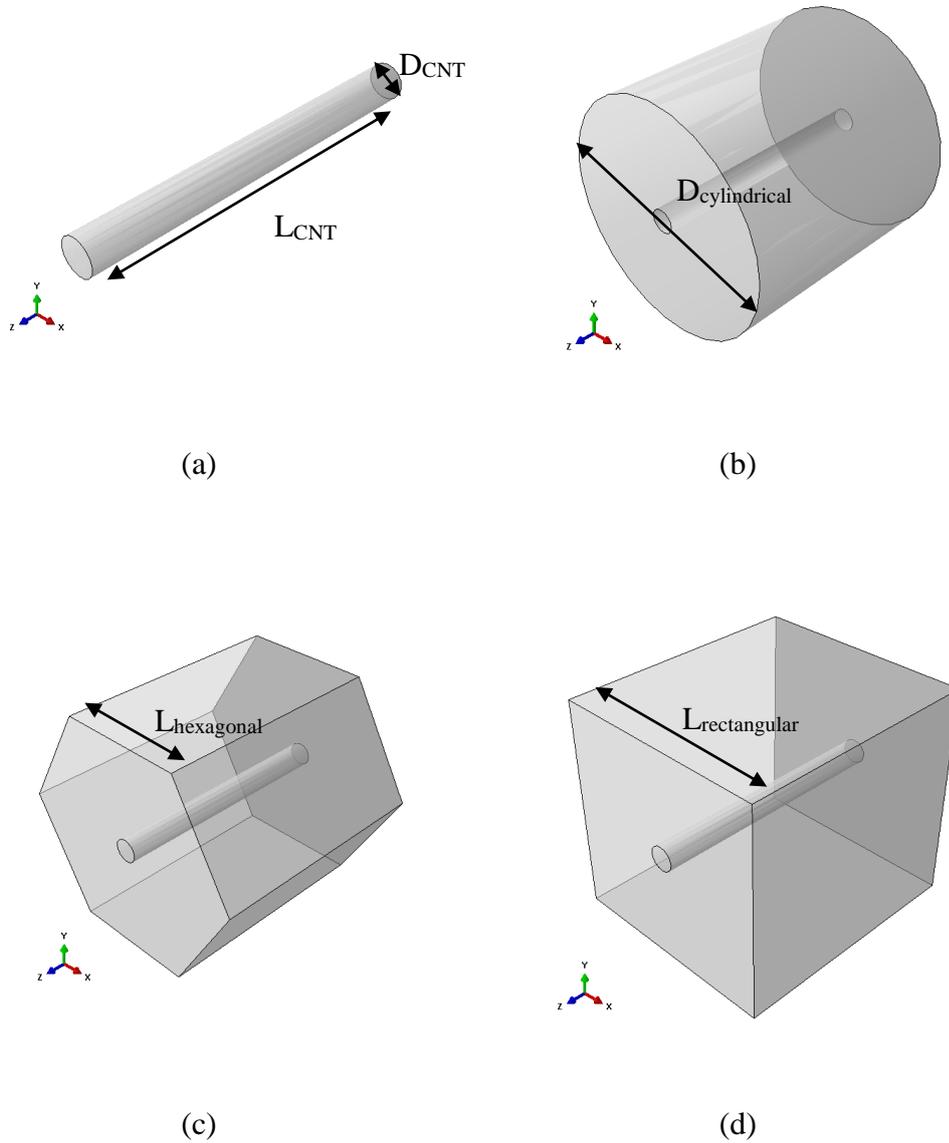


Figure 3.4 Representation of CNT and matrix a) fiber shape (same for all samples)
 b) cylindrical c) hexagonal d) rectangular shape of RVE

The homogenized elastic material constants of the samples are studied, and related results are presented in Table 3.7, Table 3.8, Table 3.9. It can be seen that there is no significant change in results according to the results.

Table 3.7 Elastic Modulus results of different RVE shapes

	E₁ [MPa]	E₂ [MPa]	E₃ [MPa]
Rectangular	4434.8	4434.2	13309.2
Cylindrical	4359.0	4358.9	12891.5
Hexagon	4441.4	4441.3	13310.5

Table 3.8 Shear Modulus results of different RVE shapes

	G₁₂ [MPa]	G₁₃ [MPa]	G₂₃ [MPa]
Rectangular	739.3	740.4	740.6
Cylindrical	736.4	725.2	725.2
Hexagon	740.6	740.4	740.4

Table 3.9 Poisson's Ratio results of different RVE shapes

	v₁₂ [-]	v₁₃ [-]	v₂₃ [-]
Rectangular	0.47	0.35	0.35
Cylindrical	0.47	0.35	0.35
Hexagon	0.47	0.35	0.35

Elastic property results for different RVE shapes can be seen in Table 3.7, Table 3.8, and Table 3.9. It can be seen that the elastic modulus values show the most remarkable change, but the change is negligible. The percentage of the difference between the mean value and the corresponding values is checked to show the difference.

Table 3.10 Percentage differences of material constants of different RVE shapes with the average values.

	E₁	E₂	E₃	G₁₂	G₁₃	G₂₃
Rectangular	0.52	0.51	1.05	0.07	0.69	0.70
Cylindrical	-1.20	-1.19	-2.12	-0.32	-1.38	-1.39
Hexagon	0.67	0.68	1.06	0.25	0.69	0.68

According to Table 3.10, the difference between results is minimal if the volume fraction is constant. The cylindrical RVE slightly underestimates the elastic constants. However, it can be concluded that any RVE shape can be chosen as long as the volume fraction is low and the same.

3.3 Effect of Fiber Placement

The effects of two different placements of fibers, i.e., CNTs, are studied in this section. In the first model, a CNT is placed entirely inside the matrix. In other words, the length of the CNT is smaller than the length of the RVE, see Figure 3.5. In the second model, the CNT and the RVE have the same length, see Figure 3.6.

The same mechanical properties shown in Table 3.6 are taken to be able to compare all results objectively. For CNT, which is completely embedded into RVE, the model and its dimensions can be seen in Figure 3.5 and Table 3.11, respectively. The ratio of fiber length to matrix length is 0.75, and the CNT volume fraction is 4%. The mesh size is chosen according to the mesh convergence study presented previously. For CNT, which is throughout RVE, the model dimensions are taken as the same in Table 3.5 for D_{CNT} , L_{CNT} , and $L_{rectangular}$.

Table 3.11 Model dimensions

w_{matrix} [nm]	h_{matrix} [nm]	L_{matrix} [nm]	D_{fiber} [nm]	L_{fiber} [nm]
76.74	76.74	133.33	10	100

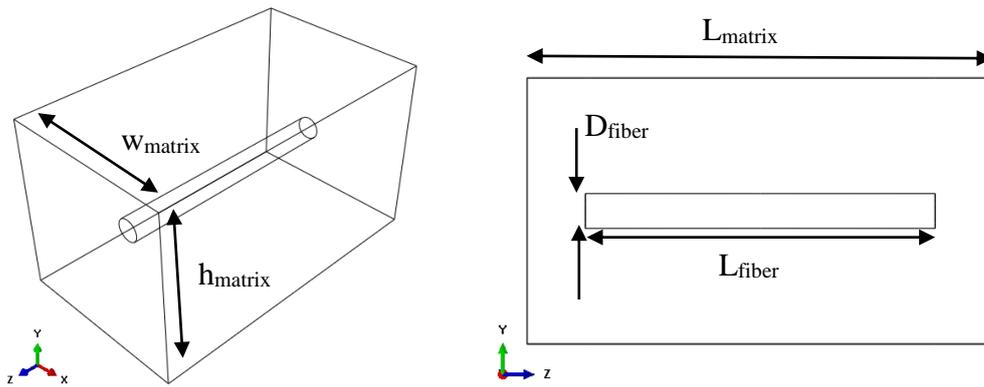


Figure 3.5 The model where the CNT is completely embedded into RVE

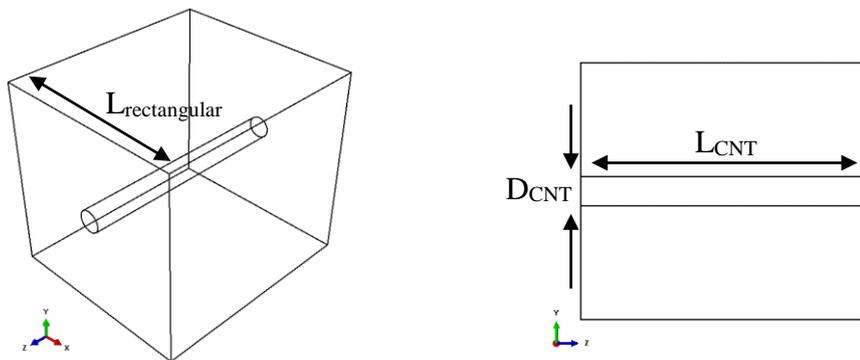


Figure 3.6 The model where the CNT is throughout RVE

The results of the two models are presented in Table 3.12. The values in the first row of Table 3.12, correspond to results of the rectangular RVE model presented in Table 3.7, Table 3.8, Table 3.9.

Table 3.12 Elastic property results of CNT throughout RVE and CNT embedded into RVE

	CNT throughout RVE	CNT embedded into RVE
E₁ [MPa]	4434.8	3856
E₂ [MPa]	4434.2	3856
E₃ [MPa]	13309.2	4679.2
G₁₂ [MPa]	739.3	697.3
G₁₃ [MPa]	740.4	700.2
G₂₃ [MPa]	740.6	700.2
ν₁₂ [-]	0.47	0.38
ν₁₃ [-]	0.35	0.35
ν₂₃ [-]	0.35	0.35

As expected, the model that has a CNT shorter than the RVE has significantly smaller Young's modulus in the direction of the CNT. Thus, the value of E_3 is very sensitive to the way how the RVE model is created. On the other hand, the other elastic parameters do not change significantly between the two models.

3.4 Embedded and Partitioned Models

In this section, homogenized material properties of RVE computed using the classical finite element method and the embedded element method are compared. In what follows, the model that is analyzed with the classical finite element method is called the partitioned model, while the other one is called the embedded model.

As stated in Chapter 2.2, there is an extra stiffness in the fiber region when the EE method is utilized since the fiber region also contains the matrix. Firstly, the stiffness of both fiber and matrix remains as it is. There will be no correction of the elastic modulus of the matrix (see Section 2.2 and Equation (2.1)). The model with no matrix property correction will be compared with the conventional partitioned model. In this way, the comparison will be objective, and both models will have the

same property but different fiber placement. Material properties are the same as given in Table 3.6. The embedded model can be seen Figure 3.7. Little yellow circles represent that the region is constrained with an embedded element.

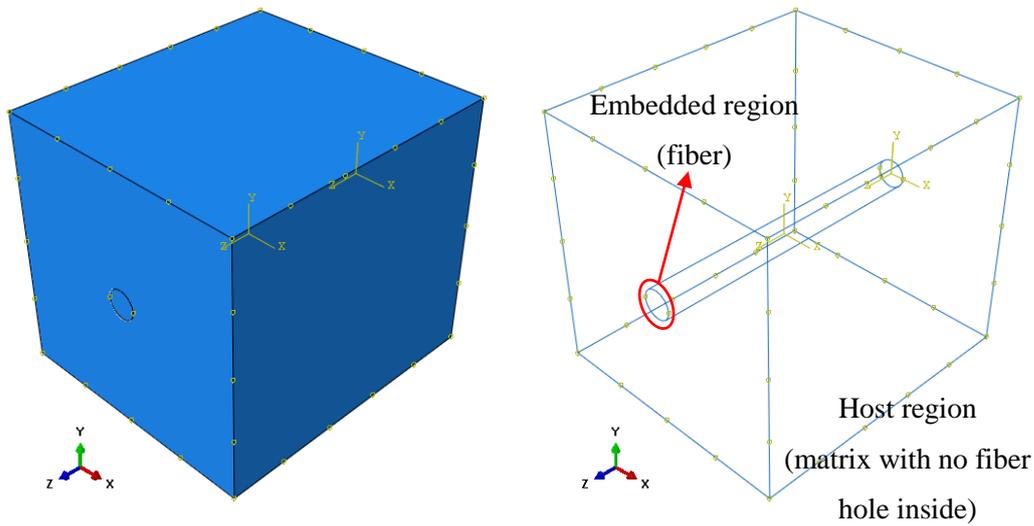


Figure 3.7 Modeling embedded and host regions in Abaqus

Table 3.13 Homogenized elastic properties for the partitioned model and the embedded model

	Rectangular Partitioned	Rectangular Embedded
E₁ [MPa]	4434.8	4725.5
E₂ [MPa]	4434.2	4745.7
E₃ [MPa]	13309.2	13975.6
G₁₂ [MPa]	739.3	764.1
G₁₃ [MPa]	740.4	764.9
G₂₃ [MPa]	740.6	760.8
v₁₂ [-]	0.47	0.47
v₁₃ [-]	0.35	0.36
v₂₃ [-]	0.35	0.35

Table 3.13 presents the results of both models. The Young's moduli and shear moduli values obtained by the embedded model are larger than the partitioned model. This result is expected since the correction of the Young's modulus value for the embedded region, i.e., CNT, is not made. Next, the elastic modulus of the CNT is corrected by subtracting the elastic modulus of the matrix, see Table 3.14, and the embedded model is reanalyzed.

Table 3.14 Reduced elastic modulus properties for CNT

	Elastic Modulus [GPa]	Poisson's Ratio [-]
CNT	996.3	0.25
Matrix	3.7	0.35

Table 3.15 Homogenized elastic properties for the partitioned model and the embedded model with reduced Young's modulus of CNT

	Rectangular Partitioned	Rectangular Embedded (Reduced E)
E₁ [MPa]	4434.8	4501.6
E₂ [MPa]	4434.2	4504.7
E₃ [MPa]	13309.2	13403.7
G₁₂ [MPa]	739.3	749.8
G₁₃ [MPa]	740.4	746
G₂₃ [MPa]	740.6	746.3
v₁₂ [-]	0.47	0.47
v₁₃ [-]	0.35	0.35
v₂₃ [-]	0.35	0.35

Table 3.15 presents the results according to the reduced elastic modulus of the CNT as shown in Table 3.14. It can be seen that difference is around 1.5% . Also, reduced fiber modulus provides the results approximate the partitioned model. It can be seen that the shear modulus and Poisson's Ratio values are closer to the partitioned model;

see Table 3.15. Therefore, reduced elastic modulus should be used for fiber in applying the embedded element method.

A similar set of analyses are conducted for RVEs where the CNT is completely inside of the RVE, i.e., the length of the CNT is shorter than the size of the RVE. The embedded model for this case is shown in Figure 3.8.

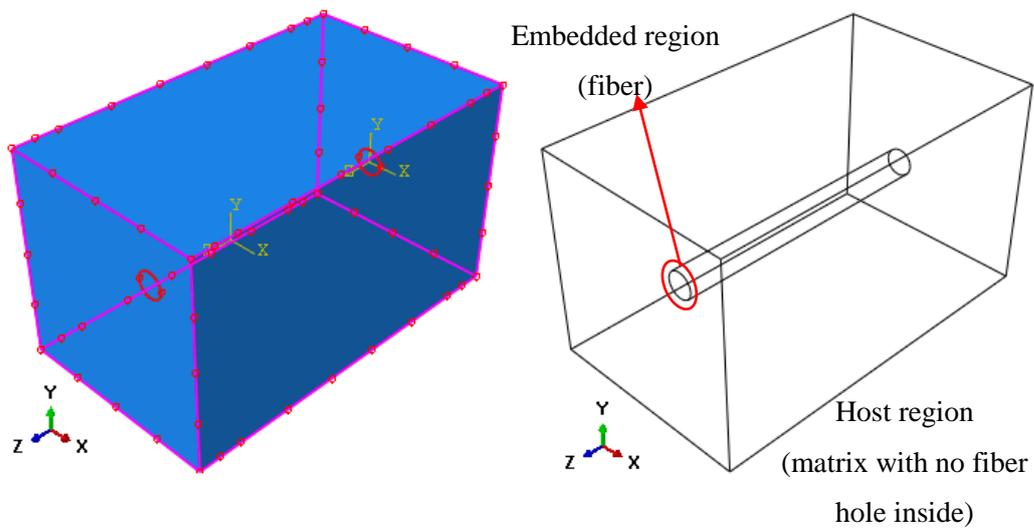


Figure 3.8 Embedded model for CNT inside of the matrix

Table 3.16 Homogenized elastic properties for the partitioned and the embedded models for CNT completely placed inside matrix

	Partitioned	Embedded
E₁ [MPa]	3856.0	3924.5
E₂ [MPa]	3856.0	3925.8
E₃ [MPa]	4679.2	4997.9
G₁₂ [MPa]	697.3	707.0
G₁₃ [MPa]	700.2	709.7
G₂₃ [MPa]	700.2	712.5
v₁₂ [-]	0.383	0.385
v₁₃ [-]	0.348	0.349
v₂₃ [-]	0.348	0.348

The homogenized elastic properties of the embedded model without correction of elastic modulus of CNT are compared with the classical partitioned model in Table 3.16 . As expected, the embedded model overestimates the partitioned model. The difference of the Young's modulus in the fiber direction, i.e., E₃, is around 6% .For E₁ and E₂ values, difference are around 1%.

Table 3.17 Homogenized elastic properties for the partitioned and the embedded models with reduced Young's modulus for CNT completely placed inside matrix

	Partitioned	Embedded (Reduced E)
E₁ [MPa]	3856.0	3896.5
E₂ [MPa]	3856.0	3898.8
E₃ [MPa]	4679.2	4754.1
G₁₂ [MPa]	697.3	704.0
G₁₃ [MPa]	700.2	706.7
G₂₃ [MPa]	700.2	711.5
v₁₂ [-]	0.383	0.385
v₁₃ [-]	0.348	0.347
v₂₃ [-]	0.348	0.348

In Table 3.17, the results of the embedded model with elastic modulus correction are presented. In this case, the maximum differences in the fiber direction modulus E_3 and the transverse modulus E_1 and E_2 are reduced to 1% and 0.9%, respectively. It can be concluded that the embedded element technique overestimates the results regardless of the CNT placement. The effect of extra stiffness around the fiber can be eliminated by distracting the elastic modulus of the matrix from the elastic modulus of the fiber.

In the following sections, the elastic modulus correction is always applied in analyses conducted with the embedded element method.

3.5 Validation with Literature

In this section, the embedded element approach used in this work is validated by a comparison with by Liu [47]. In Liu [47], the main consideration is the prediction of the effective mechanical properties of discontinuous fiber-reinforced composites. The embedded element method was used to achieve this goal. In the article, results of the classical finite element method and the embedded element method were

compared for various volume fractions of the fiber. The same model is created, and the model is reanalyzed according to the given information in the article.

A cubic RVE with a two-millimeter side is taken, and the fiber diameter is changed from 0.8 mm to 1.8 mm to change the volume fraction. The model is shown in Figure 3.9.

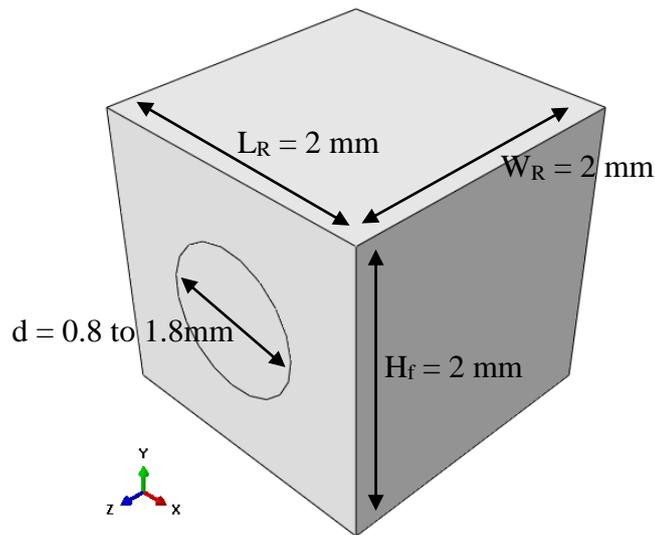


Figure 3.9 Dimensions of the model according to the article

Material properties are shown in Table 3.18. Note that the elastic modulus of the fiber is taken as 73.4 GPa for the embedded model to correct the additional stiffness.

Table 3.18 Elastic constants of the materials

	E [GPa]	ν [-]
Fiber	75	0.25
Matrix	1.6	0.35

Table 3.19 The number of mesh seeds for fiber according to fiber diameter

Fiber diameter [nm]	0.8	1	1.2	1.4	1.6	1.8
Number of mesh seeds of fiber [-]	30	38	45	53	60	68

The same mesh seeds are applied in all models for the matrix, which is 30. The mesh seeds for fiber are increased according to increasing fiber diameter to keep the element size constant. The number of mesh seeds for fiber can be seen in Table 3.19. The results in Liu [47] were presented as graphs. Note that the longitudinal elastic modulus results were very close to each other in the graph provided by article; hence, the longitudinal elastic modulus results for partitioned and the embedded element method are taken as the same. These results are digitized using WebPlotDigitizer [48] and presented in Table 3.20. Only one value is written for longitudinal elastic modulus for the embedded, and the partitioned model due to the longitudinal values clash on the graph.

Table 3.20 Results of Liu [47] digitized by WebPlotDigitizer [48]

Volume Fraction	$E_{\text{longitudinal}}$ [GPa]	$E_{\text{transverse}}$ [GPa] (Partitioned)	$E_{\text{transverse}}$ [GPa] (Embedded)
0.13	10.85	2.28	2.28
0.20	16.13	2.58	2.74
0.28	22.46	3.19	3.19
0.38	29.85	4.10	4.26
0.50	38.45	5.78	5.94
0.64	48.10	9.47	9.94

In the article, it is concluded that elastic moduli in all directions increase as volume fraction increased. Results of the traditional FE model and EE model are reasonable and close to each other.

Table 3.21 Reanalyze result of the longitudinal elastic modulus for the traditional(partitioned) model and the embedded model

Volume Fraction [%]	E_{Longitudinal}, Traditional Model [GPa]	E_{Longitudinal}, Embedded Model [GPa]
0.13	10.70	11.35
0.20	15.63	16.78
0.28	21.83	23.53
0.38	30.23	31.47
0.50	39.73	40.65
0.64	50.41	51.09

The homogenized longitudinal modulus values of the present study and Liu [47] are depicted in Table 3.21. A similar comparison for the transverse modulus is given in Table 3.22. It can be seen from these two tables that there is a good agreement between the current work and Liu [47]. The maximum differences for the longitudinal and the transverse moduli are 5% for each.

Table 3.22 Reanalyze results of the transverse elastic modulus

Volume Fraction	E_{Transverse}, Traditional Model [GPa]	E_{Transverse}, Embedded Model [GPa]
0.13	2.22	2.25
0.20	2.56	2.58
0.28	3.09	3.16
0.38	3.96	4.12
0.50	5.58	5.76
0.64	9.27	10.13

It can be seen that reanalyze results have also the same trend as the article results for transverse elastic modulus. Transverse elastic modulus results are in the range of 2% to 6%, which is conceivable.

In conclusion, the present results obtained by the embedded element method are in good agreement with Liu [47]. Thus, the current modeling approach that uses the embedded element method is validated.

CHAPTER 4

HOMOGENIZATION OF ELASTIC PROPERTIES OF CARBON NANOTUBE POLYMER COMPOSITES

By synthesizing the studies done so far, this chapter explains how the homogenization method is applied to more complicated RVEs. First, RVEs with randomly distributed unidirectional CNTs, similar to the RVE model discussed in the previous section, are examined. Then, RVEs with randomly distributed and randomly aligned CNTs are studied. Different volume fractions are also considered for these models. Furthermore, the effect of clustering of CNTs on macroscopic elastic properties is examined. In addition, the RVE size effect is also observed on the randomly distributed CNT model. Abaqus software has an interface with Python; therefore, Python code is used to create models efficiently and quickly.

4.1 Randomly Distributed Unidirectional Aligned CNTs

Previously, only a single CNT was inserted within the RVE. In this section, multiple CNTs are placed in the RVE to generate a more realistic structure. Unidirectionally aligned CNTs shows more similarity with the RVE model. Before examining the randomly distributed model of CNTs, it will be beneficial for the reliability of the method to examine the result of the homogenization method of unidirectionally distributed CNTs. Different volume fractions and multiple samples are considered to validate results.

Model dimensions can be seen in Table 4.1. Material properties are shown in Table 4.2. Model is presented in Figure 4.1. CNTs are placed unidirectionally; but randomly. This random placement of CNTs makes the structure heterogeneous.

Nevertheless, the model is expected to show mechanical properties very close to the orthotropic response obtained in the previous chapter.

Table 4.1 Model dimensions for randomly distributed unidirectional CNTs

Matrix dimensions[nm]	Fiber radius [nm]	Fiber length [nm]
34 x 34 x 34	0.34	3.4

Table 4.2 Material properties of the model

	Elastic Modulus [GPa]	Poisson's Ratio [-]
CNT	996.3	0.25
Matrix	3.7	0.35

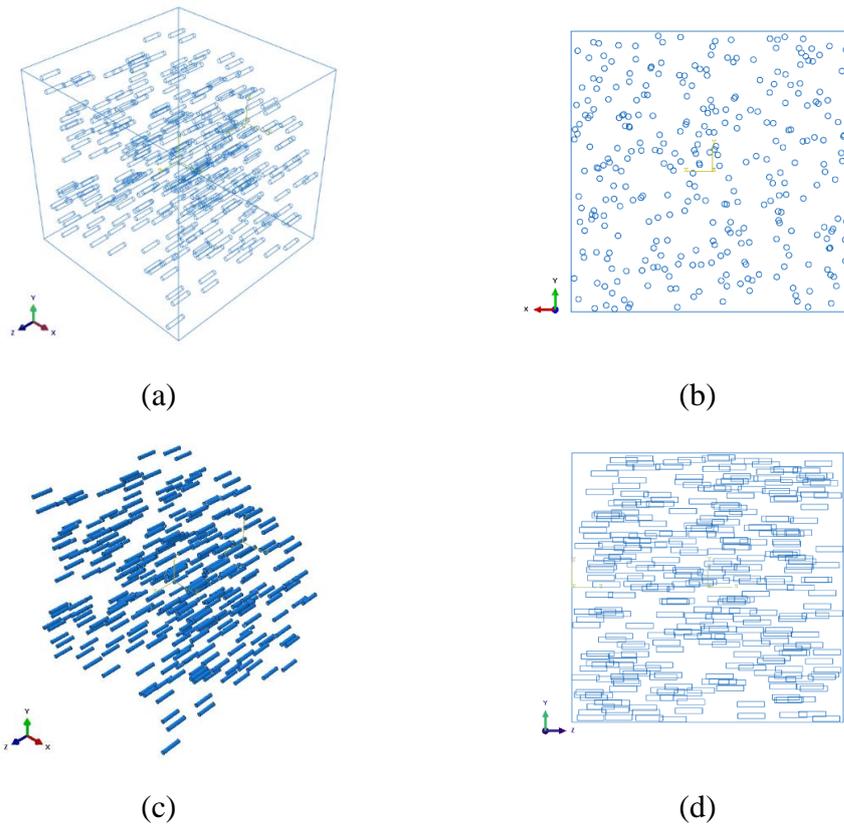


Figure 4.1 RVE with 1% randomly distributed unidirectional CNTs a) general view b) front view c) side view d) CNTs only view

The model was divided into 1000 parts so that the CNTs do not overlap. The CNTs were first generated at the origin of the model, and the generated CNTs were randomly placed in one of the dividing parts. Once a piece is filled with CNT, it can not be selected again. This procedure is repeated for each CNT with the help of Python code, see Appendix B. Number of elements for 1% and 3% models is presented in Table 4.3.

Table 4.3 Number of elements for 1% and 3% models

	1%	3%
Matrix	15625	15625
per CNT	160	160
CNTs(all)	50880	152640
Total	66505	168265

Two different volume fractions of CNTs (1% and 3%) are considered. Three different models are generated for each volume fraction. There are 318 and 954 aligned CNTs in 1% and 3% models, respectively. Related results can be seen in Table 4.4.

Table 4.4 Homogenized elastic properties of aligned CNTs for 1% and 3% volume fractions

	1%			3%		
	Sample1	Sample2	Sample3	Sample1	Sample2	Sample3
E₁ [MPa]	3863.9	3814.9	3838.4	6578.5	6432.4	6590.0
E₂ [MPa]	3879.3	3810.7	3841.6	6535.4	6466.7	6630.9
E₃ [MPa]	4787.1	4659.6	4812.3	10865.7	10709.5	10377.2
G₁₂ [MPa]	672.2	665.0	668.9	1121.7	1095.4	1147.3
G₁₃ [MPa]	730.4	717.1	725.1	1367.4	1362.2	1397.3
G₂₃ [MPa]	733.8	717.4	724.1	1402.0	1354.8	1370.1
v₁₂ [-]	0.36	0.36	0.36	0.32	0.32	0.32
v₁₃ [-]	0.33	0.33	0.33	0.30	0.30	0.29
v₂₃ [-]	0.33	0.33	0.33	0.30	0.30	0.29

As expected, E₃ values of unidirectional CNTs are greater than E₁ and E₂ values of the model. The average of E₁ and E₂ values of the all samples for 1% is 3.8 GPa. This value is 6.5 GPa for 3% model. The average of E₃ values of the all samples are 4.7 GPa and 10.6 GPa for 1% and 3% models, respectively. The difference between elastic modulus in fiber direction and the elastic modulus in transverse fiber direction is 23% and 62%, respectively. It is also expected that this difference decreases as

randomness in orientation increases. Also, results in Table 4.4 are consistent with the results reported in Table 3.17 (the model in which CNT stays completely placed inside the matrix).

4.2 Randomly Distributed CNTs

In this section, RVEs with randomly distributed and randomly oriented CNTs are studied, and homogenized elastic properties of these RVEs are computed. It should be pointed out that low volume fraction is essential for randomly dispersed CNTs; otherwise, randomness is lost in the matrix since CNT fibers tend to agglomerate when the volume fraction exceeds 3% [21]. Also, a high aspect ratio causes waviness for fiber [49]. A low aspect can avoid the waviness effect of CNT fibers.

Three different volume fractions and their effect on the whole structure will be observed. Furthermore, five different samples are generated for each volume fraction. In this way, variation of the results for different random models are checked, and the reliability of the method is controlled for low volume fractions. It is expected that mechanical properties, especially E_1 , E_2 , and E_3 , should not vary much among different random models for the same volume fraction of CNT.

The model generation is the same as randomly aligned CNTs in the previous section. At first, the matrix cube is divided into 1000 pieces as shown in Figure 4.2.

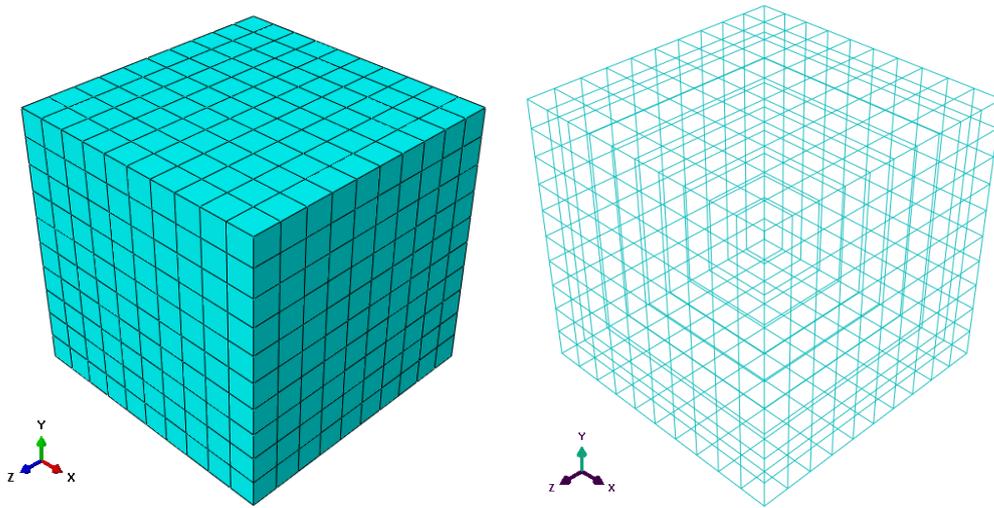


Figure 4.2 Division of the matrix into regular cubes

All CNTs are created at the origin at first. Each CNTs has different Euler angles that correspond to random orientations. At the origin, CNTs are oriented using these Euler angles. After their final orientation is determined, CNTs are randomly inserted into these small cubes (see Figure 4.2). This procedure is performed with Python code (Python code is provided in Appendix B and Appendix C). Five different random models(realizations) are created for each volume fraction. One sample for each volume fraction is presented in Figure 4.3. Three different volume fractions (1%, 2% and 3%) are considered. Table 4.5 shows the number of CNTs needed for different volume fractions. The dimensions of the CNTs and the matrix are given in Table 4.1. Dimensions are the same for all of the realizations. The only difference is their placements. Material properties of the model is given in Table 4.2.

Table 4.5 Number of fibers according to the volume fractions

Volume fraction	1%	2%	3%
Number of CNTs	318	636	954

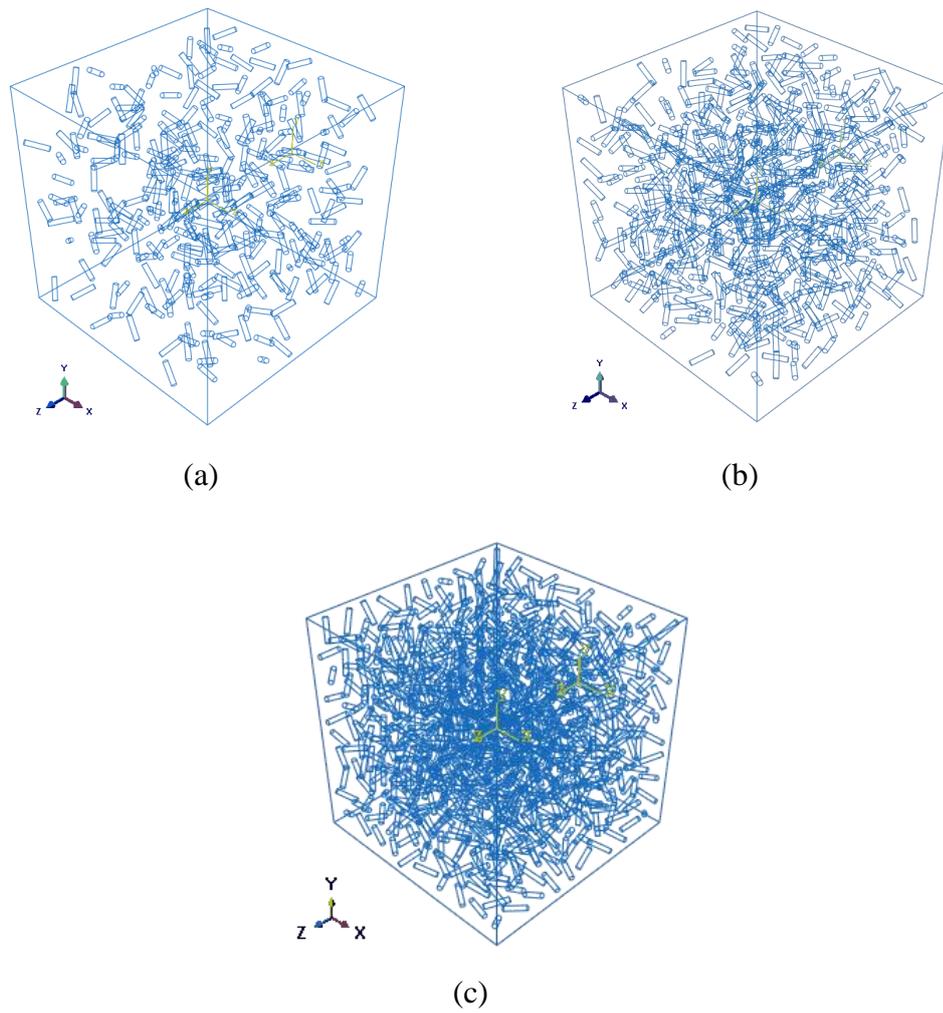


Figure 4.3 RVEs with randomly oriented CNTs for different volume fractions
 (a) 1%, (b) 2%, (c) 3%

Results for the each analysis (1%, 2% and 3%) are shown in Table 4.6, Table 4.7, Table 4.8, respectively.

Table 4.6 Elastic properties for 1% randomly distributed CNTs

	Volume Fraction 1%					
Sample #	1	2	3	4	5	avg
E₁ [GPa]	4.96	4.96	5.00	4.90	4.89	4.98
E₂ [GPa]	4.99	4.98	4.99	4.94	5.01	4.96
E₃ [GPa]	4.85	4.99	4.89	5.00	4.94	4.92
G₁₂ [GPa]	0.89	0.89	0.88	0.88	0.88	0.88
G₁₃ [GPa]	0.87	0.88	0.88	0.87	0.89	0.88
G₂₃ [GPa]	0.87	0.88	0.88	0.88	0.87	0.88
v₁₂ [-]	0.32	0.32	0.32	0.32	0.32	0.32
v₁₃ [-]	0.32	0.32	0.32	0.32	0.32	0.32
v₂₃ [-]	0.32	0.32	0.32	0.32	0.32	0.32

Table 4.7 Elastic properties for 2% randomly distributed CNTs

	Volume Fraction 2%					
Sample #	1	2	3	4	5	avg
E₁ [GPa]	7.07	7.17	7.18	7.22	6.98	7.15
E₂ [GPa]	7.10	6.99	7.20	7.15	7.19	7.15
E₃ [GPa]	7.19	7.12	7.02	7.11	7.22	7.10
G₁₂ [GPa]	1.18	1.18	1.17	1.17	1.17	1.18
G₁₃ [GPa]	1.14	1.12	1.15	1.14	1.13	1.14
G₂₃ [GPa]	1.15	1.14	1.16	1.15	1.14	1.15
v₁₂ [-]	0.29	0.28	0.28	0.28	0.28	0.28
v₁₃ [-]	0.28	0.28	0.28	0.28	0.28	0.28
v₂₃ [-]	0.28	0.28	0.29	0.28	0.28	0.28

Table 4.8 Elastic properties for 3% randomly distributed CNTs

	Volume Fraction 3%					
Sample #	1	2	3	4	5	avg
E₁ [GPa]	10.09	10.37	10.03	10.28	10.29	10.59
E₂ [GPa]	10.35	10.27	10.29	10.39	10.12	10.53
E₃ [GPa]	10.25	10.14	10.36	10.14	10.38	10.26
G₁₂ [GPa]	1.58	1.56	1.58	1.56	1.60	1.58
G₁₃ [GPa]	1.49	1.49	1.49	1.51	1.49	1.49
G₂₃ [GPa]	1.50	1.48	1.49	1.49	1.51	1.49
v₁₂ [-]	0.24	0.24	0.24	0.24	0.24	0.24
v₁₃ [-]	0.23	0.24	0.24	0.24	0.24	0.24
v₂₃ [-]	0.24	0.24	0.24	0.24	0.24	0.24

It can be seen that the elastic modulus value of the RVE varies from 4.85 GPa to 5.01 GPa for 1% volume fraction. The shear modulus value is between 0.87 GPa to 0.89 GPa. The Poisson's ratio of the samples does not show a variation and is equal to 0.32.

For 2% volume fraction case, the elastic modulus values range from 6.98 GPa to 7.22 GPa. The results for the shear modulus vary between 1.12 GPa to 1.18 GPa. The Poisson's ratio is 0.28.

The results of the elastic modulus for 3% volume fraction is between 10.09 GPa and 10.39 GPa. The shear modulus changes from 1.48 GPa to 1.60 GPa. The Poisson's ratio is found as 0.24.

The average of the three elastic moduli (E_1 , E_2 , and E_3), three shear moduli (G_{12} , G_{13} , and G_{23}) and three Poisson's ratios (v_{12} , v_{13} , and v_{23}) and the maximum differences can be seen in Table 4.9, Table 4.10, and Table 4.11.

Table 4.9 Average elastic properties and the maximum differences for 1% randomly distributed CNTs

Sample #	Volume Fraction 1%				
	1	2	3	4	5
E_{avg} [GPa]	4.93	4.98	4.96	4.94	4.95
G_{avg} [GPa]	0.88	0.88	0.88	0.88	0.88
ν_{avg} [-]	0.32	0.32	0.32	0.32	0.32
$\text{Max}(E_i-E_j)$	0.13	0.04	0.11	0.10	0.12
$\text{Max}(E_i-E_j)/E_{avg}$ [%]	2.72	0.71	2.28	2.01	2.41
$\text{Max}(G_i-G_j)$	0.02	0.01	0.01	0.01	0.01
$\text{Max}(G_i-G_j)/G_{avg}$ [%]	2.13	0.87	0.76	1.54	1.40

Table 4.10 Average elastic properties and the maximum differences for 2% randomly distributed CNTs

Sample #	Volume Fraction 2%				
	1	2	3	4	5
E_{avg} [GPa]	7.12	7.09	7.13	7.16	7.13
G_{avg} [GPa]	1.16	1.15	1.16	1.15	1.15
ν_{avg} [-]	0.28	0.28	0.28	0.28	0.28
$\text{Max}(E_i-E_j)$	0.12	0.17	0.18	0.10	0.24
$\text{Max}(E_i-E_j)/E_{avg}$ [%]	1.73	2.44	2.55	1.44	3.33
$\text{Max}(G_i-G_j)$	0.04	0.05	0.02	0.03	0.03
$\text{Max}(G_i-G_j)/G_{avg}$ [%]	3.98	5.46	1.79	2.91	2.89

Table 4.11 Average elastic properties and the maximum differences for 3% randomly distributed CNTs

Sample #	Volume Fraction 3%				
	1	2	3	4	5
E_{avg} [GPa]	10.23	10.26	10.23	10.27	10.26
G_{avg} [GPa]	1.53	1.51	1.52	1.52	1.53
ν_{avg} [-]	0.24	0.24	0.24	0.24	0.24
$\text{Max}(E_i-E_j)$	0.26	0.23	0.33	0.25	0.26
$\text{Max}(E_i-E_j)/E_{avg}$ [%]	2.51	2.28	3.24	2.41	2.57
$\text{Max}(G_i-G_j)$	0.06	0.05	0.06	0.05	0.06
$\text{Max}(G_i-G_j)/G_{avg}$ [%]	5.77	4.92	5.76	4.63	5.77

The variation of the elastic properties in different directions is very low, and hence, the responses could be considered isotropic. Furthermore, the variations among different realizations are also at an acceptable level. As expected, the elastic constants increase with increasing volume fraction. In comparison to the elastic modulus values (E_1 , E_2 , and E_3), the shear moduli (G_{12} , G_{13} , and G_{23}) and the Poisson's ratios (ν_{12} , ν_{13} , and ν_{23}) show much less variation both in different directions and also among different realizations.

4.3 The Effect of Number of Randomly Oriented CNTs

This section studies the effect of the number of randomly distributed CNTs on the homogenized elastic properties of RVEs. Since, in reality, nanocomposites have a very large number of inclusions, a study on the minimum number of CNTs in a representative RVE is needed. It is obvious that an RVE including a single CNT does not properly represent the whole heterogeneous structure. Therefore, the acceptable number of CNTs in the RVE should be determined. In this section, several models are created by changing the number of CNTs while keeping the volume fraction constant. In this way, as the number of CNTs increases, the heterogeneity of the

structure will be more accurately represented; however, it is also not reasonable to pick an RVE, including a great number of CNTs in terms of modeling and computation time.

First, an RVE with a single CNT is created. The CNT has a length of 3.4 nm and a diameter of 0.34 nm. Then, the total number of CNTs is increased while keeping the dimensions of each CNT constant. The RVE sizes are changed to keep the volume fraction constant. The total number of CNTs are increased from 1 to 400. Five different random models are analyzed for each RVE size that has different number of CNTs. Mesh sizes are also kept constant in all models so that the only variable is the number of CNTs. Samples from the models are shown in Figure 4.4. The total number of CNTs changes for each different matrix. The volume fraction is chosen as 1%.

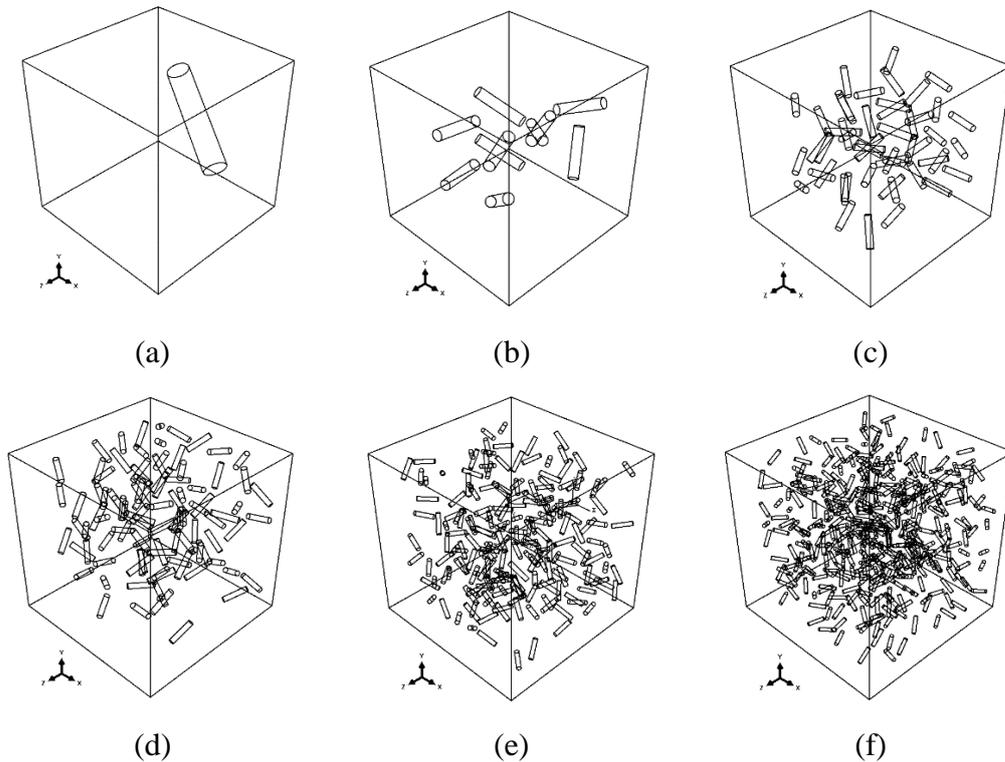


Figure 4.4 Sample models for different number of CNTs a) 1, b) 10, c) 50, d) 100, e) 200, f) 400 CNTs. The volume fraction is 1% in all models.

Material properties are taken the same, see Table 4.2. and the same boundary conditions are applied to the models to provide consistency. The same Python code is utilized to create models, and process the analysis data.

The elastic modulus values (E_1 , E_2 , and E_3) and the shear modulus values (G_{12} , G_{13} , and G_{23}) are averaged for each model. Averaging includes all values found from the samples for elastic modulus and shear modulus, separately. Equations (4.1) and (4.2) explain the averaging procedure.

$$\bar{E} = \frac{1}{3 N_R} \sum_{n=1}^{N_R} \sum_{i=1}^3 E_i^n \quad (4.1)$$

$$\bar{G} = \frac{1}{3 N_R} \sum_{n=1}^{N_R} (G_{12} + G_{23} + G_{13})^n \quad (4.2)$$

N_R , \bar{E} and \bar{G} stand for the number of realizations, the average elastic modulus, and the average shear modulus, respectively.

Figure 4.5 and Figure 4.6 show the variation of the elastic and the shear moduli with the increasing number of CNTs.

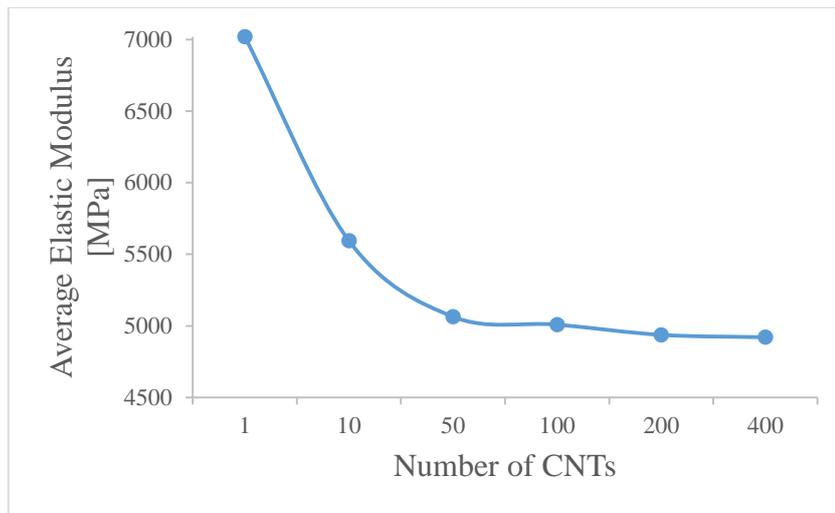


Figure 4.5 Average Elastic Modulus vs Number of CNTs for 1% volume fraction

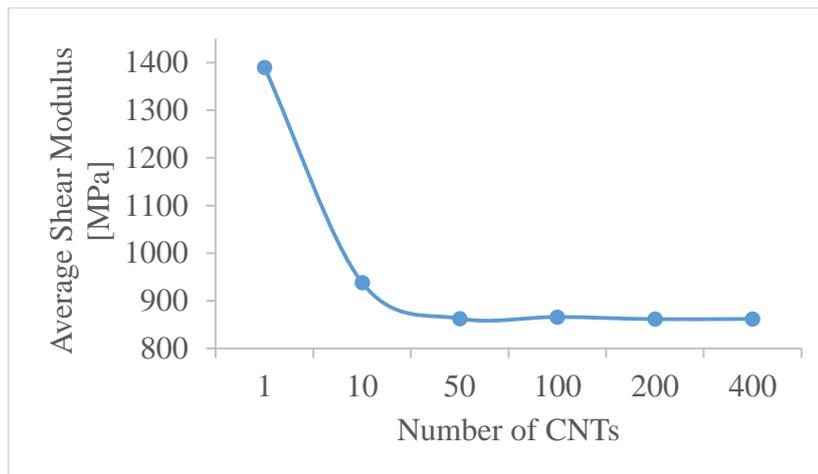


Figure 4.6 Average shear modulus vs number of CNTs for 1% volume fraction

As expected, the model including only one fiber is not enough to represent the whole model correctly. As the number of CNTs increases, the results seem to converge to a value. After 100 CNTs, the elastic modulus does not change much, while this threshold is 50 CNTs for the shear modulus.

It should be noted that the convergence result obtained here is valid for the particular matrix-fiber pair. In other words, for different matrix-fiber pairs where the ratio of elastic moduli of two phases is significantly different from the present case, the minimum number of fibers for convergence could be different. A similar limitation is also true for fibers with different aspect ratios.

The mean percentage difference shows the average deviation of the results. The maximum difference between elastic modulus values (E_1 , E_2 , and E_3) is calculated for each realization. Then, these values are averaged over the number of realizations. Finally, the obtained values are normalized with mean value \bar{E} . The same computations are done for the shear modulus, too. The mean percentage difference is calculated in Equations (4.3) and (4.4). The number of realizations is indicated by n . Values from five different realizations are considered. Hence, n is taken 5.

$$\Delta E_{MPD} = \frac{1}{n} \sum_{i=1}^n \frac{\max(E_1^i, E_2^i, E_3^i) - \min(E_1^i, E_2^i, E_3^i)}{\bar{E}} \quad (4.3)$$

$$\Delta G_{MPD} = \frac{1}{n} \sum_{i=1}^n \frac{\max(G_{12}^i, G_{23}^i, G_{13}^i) - \min(G_{12}^i, G_{23}^i, G_{13}^i)}{\bar{E}} \quad (4.4)$$

Figure 4.7 and Figure 4.8 show the percentage difference for the elastic and the shear moduli.

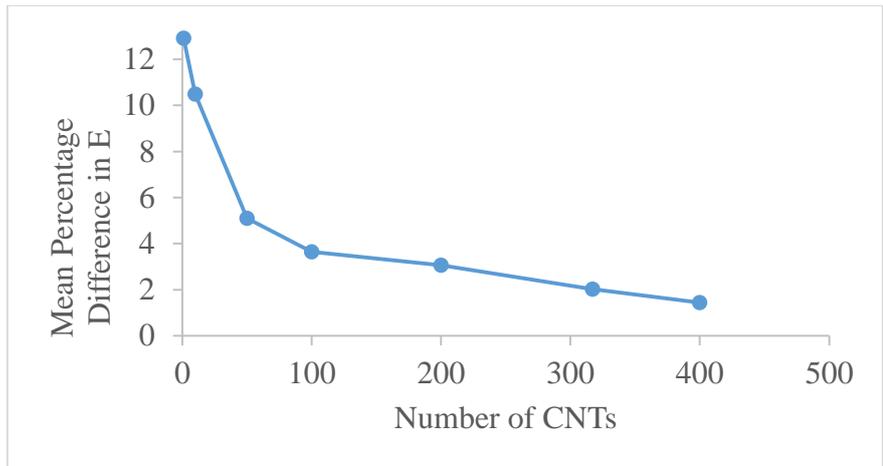


Figure 4.7 The mean percentage difference for elastic modulus for different number of CNTs

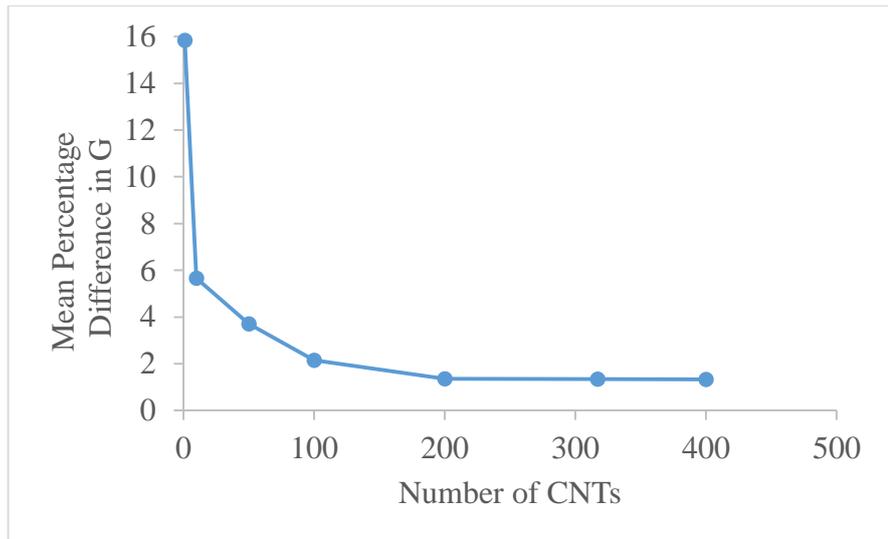


Figure 4.8 The mean percentage difference for shear modulus for different number of CNTs

Figure 4.7 and Figure 4.8 exhibit a similar trend with Figure 4.5 and Figure 4.6. As the number of CNTs increases, variations among different realizations vanish. However, the main purpose is to represent the heterogeneous material property with

a small number of CNTs. Therefore, an optimal value can be chosen around 100 CNTs.

The worst-case for the different number of CNTs are also computed. In this case, instead of averaging the results, the maximum difference is chosen for the worst percentage difference. The worst percentage difference values E_WPD and G_WPD are computed as follows.

$$\Delta E_{WPD} = \max_n \left[\frac{\max(E_1^n, E_2^n, E_3^n) - \min(E_1^n, E_2^n, E_3^n)}{\bar{E}} \right] \quad (4.5)$$

$$\Delta G_{WPD} = \max_n \left[\frac{\max(G_{12}^n, G_{23}^n, G_{13}^n) - \min(G_{12}^n, G_{23}^n, G_{13}^n)}{\bar{E}} \right] \quad (4.6)$$

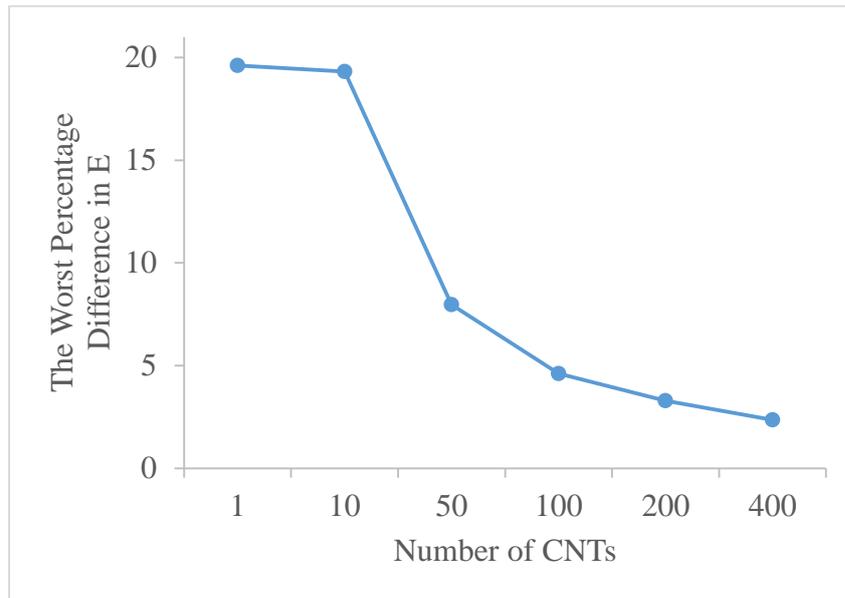


Figure 4.9 The worst percentage difference for elastic modulus for different number of CNTs

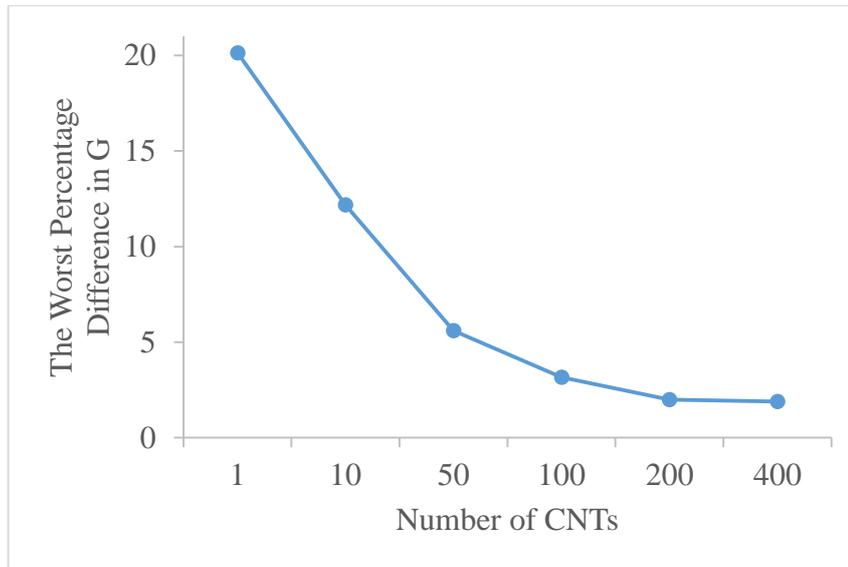


Figure 4.10 The worst percentage difference for shear modulus for different number of CNTs

As expected, the worst percentage difference is greater than the mean percentage difference. However, the change can be considered negligible. The results converge for 100 and 50 CNTs for the elastic and the shear moduli, respectively. The maximum difference for the elastic modulus is 4.6% with 100 CNTs. This value is 5.59% for the shear modulus for 50 CNTs. Since the optimal results are desired, it can be concluded that an RVE should contain at least 100 CNTs for homogenization procedure.

4.4 The Effect of Clustering on the Elastic Properties

It is well known that CNTs in the matrix begin to agglomerate after a certain ratio [21]. Clustering in the structure could deteriorate the mechanical performance of the composite. In this section, the effect of clustering on the homogenized elastic properties of nano-composites is studied.

3×3, 4×4, and 5×5 cluster models are created to examine this effect. To create a cluster, first, a random cube is selected. CNTs are then placed in the first cube and

the neighboring cubes around the first cube. After creation of a cluster of a given size, the remaining CNTs are randomly placed into the RVE. The clusters can not be visualized easily for large volume fractions since the matrix is nearly occupied with CNTs. Therefore, 1% volume fraction case is studied for each cluster model. However, 2% and 3% volume fractions are also studied for 3×3 cluster model (for details, see Appendix D). Five different random samples are analyzed for each cluster models.

CNT cluster models can be seen in Figure 4.11, Figure 4.12, and Figure 4.13.

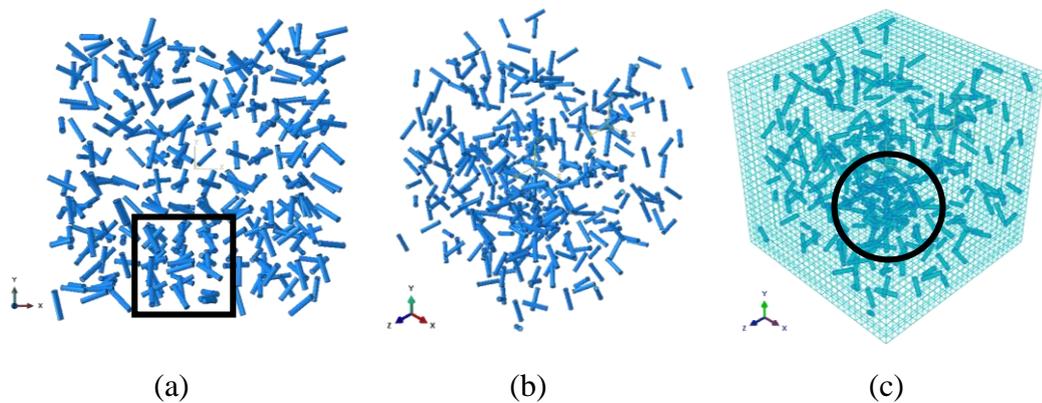


Figure 4.11 3×3 Cluster model sample for 1% volume fraction a) side view of CNTs, b) iso view of CNTs, c) whole model

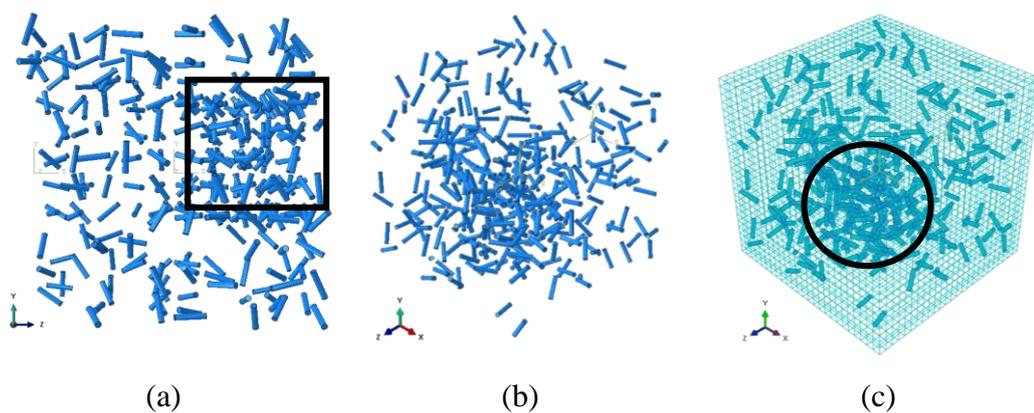


Figure 4.12 4×4 Cluster model sample for 1% volume fraction a) side view of CNTs, b) iso view of CNTs, c) whole model

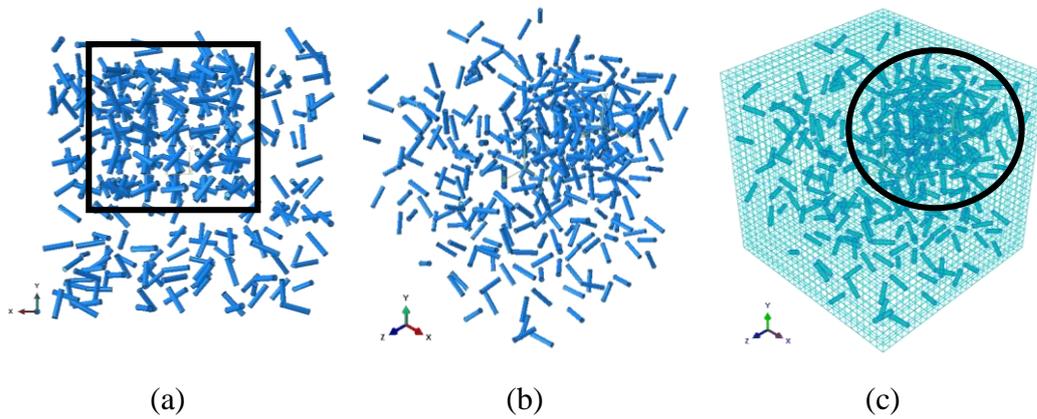


Figure 4.13 5×5 Cluster model sample for 1% volume fraction a) side view of CNTs, b) iso view of CNTs, c) whole model

Material properties are chosen the same as given in Table 4.2, and the same boundary conditions are applied to the models. In brief, the only change is the selected cluster cubes so that cluster effects can be compared objectively.

Results are shown for three different cluster models with 1% volume fractions in Table 4.12, Table 4.13, and Table 4.14.

Table 4.12 Homogenized elastic properties for five different 3×3 cluster models with volume fraction of 1%

sample #	1	2	3	4	5	avg
E₁ [MPa]	5021	4994	4976	5000	4944	4987
E₂ [MPa]	4930	5041	4997	5067	4970	5001
E₃ [MPa]	5015	5004	4939	5005	5004	4993
G₁₂ [MPa]	896	880	877	886	884	885
G₁₃ [MPa]	875	887	880	873	885	880
G₂₃ [MPa]	879	881	879	883	882	881
v₁₂ [-]	0.32	0.32	0.32	0.32	0.32	0.32
v₁₃ [-]	0.32	0.32	0.32	0.32	0.33	0.32
v₂₃ [-]	0.32	0.32	0.32	0.32	0.32	0.32

Table 4.13 Homogenized elastic properties for five different 4×4 cluster models with volume fraction of 1%

Sample #	1	2	3	4	5	avg
E₁ [MPa]	5108	5215	5057	5191	5179	5050
E₂ [MPa]	5134	5038	5096	5053	5129	5090
E₃ [MPa]	4980	5035	5048	5030	5013	5021
G₁₂ [MPa]	910	902	889	896	908	901
G₁₃ [MPa]	890	885	885	888	885	887
G₂₃ [MPa]	886	891	877	888	889	886
v₁₂ [-]	0.32	0.31	0.32	0.31	0.32	0.32
v₁₃ [-]	0.32	0.31	0.32	0.31	0.32	0.32
v₂₃ [-]	0.32	0.33	0.32	0.33	0.32	0.32

Table 4.14 Homogenized elastic properties for five different 5×5 cluster models with volume fraction of 1%

Sample #	1	2	3	4	5	avg
E₁ [MPa]	5139	5169	5157	5030	5067	5112
E₂ [MPa]	5212	5162	5223	5150	5122	5174
E₃ [MPa]	5010	5118	5028	5083	5314	5111
G₁₂ [MPa]	900	905	901	892	899	899
G₁₃ [MPa]	866	865	870	857	869	865
G₂₃ [MPa]	863	866	866	856	865	863
v₁₂ [-]	0.32	0.31	0.32	0.32	0.31	0.32
v₁₃ [-]	0.32	0.31	0.32	0.32	0.31	0.32
v₂₃ [-]	0.31	0.32	0.31	0.31	0.32	0.31

It can be seen that elastic properties tend to increase as cluster region increases. Also, the small cluster in the matrix (like 3×3 cluster model) does not significantly affect the structure.

The percentage difference between elastic property values of the cluster models and the random model results (Table 4.6) can be seen in Table 4.15. The percentage difference is calculated by using the average values of the five different samples of the cluster and that of the random model.

Table 4.15 Percentage difference between cluster models and the random model (no cluster) results

	3×3	4×4	5×5
E₁	0.93	2.22	3.46
E₂	0.38	2.17	3.85
E₃	1.18	1.74	3.56
G₁₂	0.04	1.89	1.71
G₁₃	0.31	1.08	-1.38
G₂₃	0.42	1.01	-1.62
v₁₂	-0.35	-1.60	-1.60
v₁₃	-0.07	-1.93	-1.93
v₂₃	-0.79	0.45	-2.65

As stated before, when the level of agglomeration increases, the elastic moduli tend to increase monotonously. The variation of the shear moduli and the Poisson's ratio with cluster size is non-monotonous. It seems that they depend not only on the size of the cluster but also on the location of the cluster.

Larger cluster sizes are not studied since it is not possible to model them with the current RVE size. Larger RVEs are needed to study bigger clusters.

CHAPTER 5

CONCLUSION AND FUTURE WORK

The objective of the thesis is to determine the elastic properties of the polymer nanocomposites by computational homogenization using the embedded element method. First, the embedded element method is validated by comparing the homogenized elastic properties obtained by the embedded element method with the results of the conventional finite element method.

The effect of RVE shape on the results was studied. It was found that the RVE shape does not affect the homogenized properties significantly. It was concluded that any RVE shape could be used, as long as the volume fraction is kept the same. Rectangular RVE shape was preferred in this study for its simplicity.

The effect of fiber placement was studied by considering two different models. CNT was placed throughout the RVE and embedded into the RVE. The elastic modulus along the CNT direction was found 200% greater than that of the transverse direction in CNT throughout RVE. It is only 21% greater in the case of the embedded model. It was concluded that CNT embedded into RVE represents heterogeneous material better for the homogenization process.

The difference between the embedded and the traditional partitioned finite element models were studied. It was found that the embedded model adds extra stiffness to the system due the overlapping regions of matrix and CNT. As a result, the elastic constants were found greater for the embedded model. The extra stiffness was eliminated by subtracting the elastic modulus of the matrix from the elastic modulus of the CNT.

An RVE with a single CNT does not represent the nano-composite material properly. Therefore, RVEs with many randomly placed and randomly oriented CNTs were created. Since random models were examined, more samples needed to be examined

to verify results. Therefore, five different random realizations were made for each volume fraction.

The minimum number of CNTs required in RVEs was determined to obtain a converged homogenized elastic properties. The number of CNTs in the RVE was increased while keeping the volume fraction constant. It was observed that the results converged for RVEs containing approximately 100 CNTs or more. It is important to note that the result obtained here regarding the minimum number of CNTs is valid for the particular matrix-fiber pair. For different matrix-fiber pairs with different mechanical properties, the minimum number of fibers for convergence could be different. A similar limitation is also true for CNTs with different aspect ratios.

Since CNTs have an agglomeration problem, the effect of small clusters of CNTs on the model was examined for three different cluster sizes. The results showed that clusters increase the Young's modulus monotonously in the range of cluster sizes investigated. It was seen that small clusters did not affect the result significantly.

In this study, the embedded element technique was used for computational homogenization. In the homogenization analyses, displacement boundary conditions were considered only. Periodic boundary conditions and uniform traction boundary conditions can also be used, and the results could be compared.

The RVEs created in this study do not allow CNTs to touch the boundaries and go beyond them. This type of more complex RVEs could be created and studied.

REFERENCES

- [1] S. Iijima, "Helical microtubules of graphitic carbon," *Nature*, 1991, doi: 10.1038/354056a0.
- [2] B. D. Malhotra, S. Srivastava, and S. Augustine, "Biosensors for food toxin detection: Carbon nanotubes and graphene," 2015, doi: 10.1557/opl.2015.165.
- [3] D. Heider, G. Pandey, and E. T. Thostenson, "(12) United States Patent," vol. 1, no. 12, 2016.
- [4] "Piranha USV Concept – Zyv Tech." .
- [5] "Sports — Zyvex Technologies." .
- [6] J. C. Moses, A. Gangrade, and B. B. Mandal, "Carbon Nanotubes and Their Polymer Nanocomposites," in *Nanomaterials and Polymer Nanocomposites: Raw Materials to Applications*, 2018.
- [7] K. Iakoubovskii, "Techniques of aligning carbon nanotubes," *Central European Journal of Physics*. 2009, doi: 10.2478/s11534-009-0072-2.
- [8] M. Cieřla and P. Kubala, "Random sequential adsorption of cuboids," *J. Chem. Phys.*, vol. 149, no. 19, p. 194704, Nov. 2018, doi: 10.1063/1.5061695.
- [9] M. M. Shokrieh and R. Rafiee, "On the tensile behavior of an embedded carbon nanotube in polymer matrix with non-bonded interphase region," *Compos. Struct.*, 2010, doi: 10.1016/j.compstruct.2009.09.033.
- [10] X. L. Chen and Y. J. Liu, "Square representative volume elements for evaluating the effective material properties of carbon nanotube-based composites," *Comput. Mater. Sci.*, 2004, doi: 10.1016/S0927-0256(03)00090-9.

- [11] N. Hu, H. Fukunaga, C. Lu, M. Kameyama, and B. Yan, "Prediction of elastic properties of carbon nanotube reinforced composites," *Proc. R. Soc. A Math. Phys. Eng. Sci.*, 2005, doi: 10.1098/rspa.2004.1422.
- [12] G. M. Odegard, T. S. Gates, K. E. Wise, C. Park, and E. J. Siochi, "Constitutive modeling of nanotube-reinforced polymer composites," *Compos. Sci. Technol.*, 2003, doi: 10.1016/S0266-3538(03)00063-0.
- [13] Y. J. Liu and X. L. Chen, "Evaluations of the effective material properties of carbon nanotube-based composites using a nanoscale representative volume element," *Mech. Mater.*, 2003, doi: 10.1016/S0167-6636(02)00200-4.
- [14] Z. Hu, M. R. H. Arefin, X. Yan, and Q. H. Fan, "Mechanical property characterization of carbon nanotube modified polymeric nanocomposites by computer modeling," *Compos. Part B Eng.*, 2014, doi: 10.1016/j.compositesb.2013.08.052.
- [15] Z. Lu, Z. Yuan, Q. Liu, Z. Hu, F. Xie, and M. Zhu, "Multi-scale simulation of the tensile properties of fiber-reinforced silica aerogel composites," *Mater. Sci. Eng. A*, 2015, doi: 10.1016/j.msea.2014.12.007.
- [16] Z. Lu, Z. Yuan, and Q. Liu, "3D numerical simulation for the elastic properties of random fiber composites with a wide range of fiber aspect ratios," *Comput. Mater. Sci.*, 2014, doi: 10.1016/j.commatsci.2014.04.007.
- [17] A. Awasthi, R. Sharma, and R. Ghosh, "Application of Embedded Element Approach to Nanostructure of Bone," 2018.
- [18] A. Matveeva, V. Romanov, S. Lomov, and L. Gorbatikh, "Application of the embedded element technique to the modelling of nano-engineered fiber-reinforced composites," 2015.
- [19] V. S. Romanov, "Modeling tools for micro-scale stress analysis of nano-engineered fiber-reinforced composites," 2015.
- [20] Zohdi, Tarek I. and P. Wriggers, *An Introduction to Computational*

Micromechanics, First Edit. Springer, 2005.

- [21] R. I. Rubel, M. H. Ali, M. A. Jafor, and M. M. Alam, “Carbon nanotubes agglomeration in reinforced composites: A review,” *AIMS Materials Science*, vol. 6, no. 5. 2019, doi: 10.3934/matersci.2019.5.756.
- [22] F. Montero and F. Medina, “Determination of the RVE size of quasi-brittle materials using the discrete element method,” in *Particle-Based Methods II - Fundamentals and Applications*, 2011, pp. 391–402, [Online]. Available: [https://upcommons.upc.edu/bitstream/handle/2117/189093/Particles_2011-38_Determination of the RVE size.pdf?sequence=1&isAllowed=y](https://upcommons.upc.edu/bitstream/handle/2117/189093/Particles_2011-38_Determination%20of%20the%20RVE%20size.pdf?sequence=1&isAllowed=y).
- [23] ABAQUS, “Abaqus 6.14 Documentation,” *Abaqus 6.14 Anal. User’s Guid.*, 2014.
- [24] “Abaqus Documentation MIT.” <https://abaqus-docs.mit.edu/2017/English/SIMACAECSTRefMap/simacst-c-embeddedelement.htm>.
- [25] Eshelby JD., “The determination of the elastic field of an ellipsoidal inclusion, and related problems,” *Proc. R. Soc. London. Ser. A. Math. Phys. Sci.*, vol. 241, no. 1226, pp. 376–396, Aug. 1957, doi: 10.1098/rspa.1957.0133.
- [26] Y. Benveniste, “A new approach to the application of Mori-Tanaka’s theory in composite materials,” *Mech. Mater.*, vol. 6, no. 2, pp. 147–157, Jun. 1987, doi: 10.1016/0167-6636(87)90005-6.
- [27] P. R. Budarapu, X. Zhuang, T. Rabczuk, and S. P. A. Bordas, *Multiscale modeling of material failure: Theory and computational methods*, 1st ed., vol. 52. Elsevier Inc., 2019.
- [28] S. Belhouideg, “Prediction of effective mechanical properties of composite materials using homogenization approach: Application to tungsten fiber reinforced bulk metallic glass matrix composite,” *Eur. Mech. Sci.*, vol. 2, no.

2, pp. 68–75, Jun. 2018, doi: 10.26701/ems.376369.

- [29] H. J. Böhm, “Continuum Micromechanics of Materials,” no. December, p. 104, 2010, [Online]. Available: https://www.researchgate.net/publication/268339214_CONTINUUM_MICROMECHANICS_OF_MATERIALS.
- [30] S. Kari, H. Berger, and U. Gabbert, “Numerical evaluation of effective material properties of randomly distributed short cylindrical fibre composites,” *Comput. Mater. Sci.*, vol. 39, no. 1, pp. 198–204, Mar. 2007, doi: 10.1016/J.COMMATSCI.2006.02.024.
- [31] I. Temizer, “Micromechanics Analysis of Heterogeneous Materials,” 2012. [Online]. Available: <http://imechanica.org/node/12852>.
- [32] A. J. A. Morgan, “Higher Order Tensors.,” *SIAM J. Appl. Math.*, vol. 30, no. 2, pp. 355–380, 1976, doi: 10.1137/0130035.
- [33] Y. Shapira, “The Linear Elasticity Equations,” in *Solving PDEs in C++*, 2011, pp. 403–412.
- [34] N. Tiwari, “Mechanics of Laminated Composite Structures Lecture 13 Analysis of a Laminated Composite.” [Online]. Available: <https://nptel.ac.in/content/storage2/courses/112104168/L22.pdf>.
- [35] A. Bertei, C. C. Chueh, J. G. Pharoah, and C. Nicolella, “Modified collective rearrangement sphere-assembly algorithm for random packings of nonspherical particles: Towards engineering applications,” *Powder Technol.*, 2014, doi: 10.1016/j.powtec.2013.11.034.
- [36] K. Thomas, H. C. A. Bryce, and M. Heitzmann, “Generation of a short fibre biocomposite representative volume element,” 2016, doi: 10.14264/uql.2016.500.
- [37] H. J. Böhm, A. Eckschlager, and W. Han, “Multi-inclusion unit cell models for metal matrix composites with randomly oriented discontinuous

- reinforcements,” *Comput. Mater. Sci.*, vol. 25, no. 1–2, pp. 42–53, Sep. 2002, doi: 10.1016/S0927-0256(02)00248-3.
- [38] Y. Pan, L. Iorga, and A. A. Pelegri, “Analysis of 3D random chopped fiber reinforced composites using FEM and random sequential adsorption,” *Comput. Mater. Sci.*, vol. 43, no. 3, pp. 450–461, Sep. 2008, doi: 10.1016/J.COMMATSCI.2007.12.016.
- [39] Y. Pan, L. Iorga, and A. A. Pelegri, “Numerical generation of a random chopped fiber composite RVE and its elastic properties,” *Compos. Sci. Technol.*, vol. 68, no. 13, pp. 2792–2798, Oct. 2008, doi: 10.1016/J.COMPSCITECH.2008.06.007.
- [40] D. Duschlbauer, H. J. Böhm, and H. E. Pettermann, “Computational simulation of composites reinforced by planar random fibers: Homogenization and localization by unit cell and mean field approaches,” *J. Compos. Mater.*, vol. 40, no. 24, pp. 2217–2234, Dec. 2006, doi: 10.1177/0021998306062317.
- [41] W. Zhang, “Experimental and Computational Analysis of Random Cylinder Packings With Applications,” Louisiana State University, 2006.
- [42] H. Altendorf and D. Jeulin, “Random-walk-based stochastic modeling of three-dimensional fiber systems,” *Phys. Rev. E*, vol. 83, no. 4, p. 041804, Apr. 2011, doi: 10.1103/PhysRevE.83.041804.
- [43] J. Zhou, L. Qi, and A. M. Gokhale, “Generation of Three-Dimensional Microstructure Model for Discontinuously Reinforced Composite by Modified Random Sequential Absorption Method,” *J. Eng. Mater. Technol. Trans. ASME*, vol. 138, no. 2, pp. 1–8, 2016, doi: 10.1115/1.4032152.
- [44] R. Lakes, “Viscoelastic Composite Materials,” *Viscoelastic Materials*, 2010. <http://silver.neep.wisc.edu/~lakes/VECmp.html>.
- [45] C. L. Cheung, A. Kurtz, H. Park, and C. M. Lieber, “Diameter-controlled

synthesis of carbon nanotubes,” *J. Phys. Chem. B*, 2002, doi:
10.1021/jp0142278.

- [46] “Properties Supplier Data - Polyetheretherketone (PEEK).” [Online].
Available: <https://www.azom.com/properties.aspx?ArticleID=1882>.
- [47] H. Liu, D. Zeng, Y. Li, and L. Jiang, “Development of RVE-embedded solid elements model for predicting effective elastic constants of discontinuous fiber reinforced composites,” *Mech. Mater.*, 2016, doi:
10.1016/j.mechmat.2015.10.011.
- [48] “WebPlotDigitizer.” <https://apps.automeris.io/wpd/>.
- [49] A. Chanteli and K. I. Tserpes, “Finite element modeling of carbon nanotube agglomerates in polymers,” *Compos. Struct.*, vol. 132, 2015, doi:
10.1016/j.compstruct.2015.07.033.

APPENDICES

A. Sample Python Code for Averaging Calculations

Sample Python code is provided for averaging calculations. X displacement calculations are shown to represent methodology. A similar procedure is done for y and z displacements.

```
import sys
from odbAccess import *
from abaqusConstants import*
from types import IntType
import numpy as np
#openMdb('spherical_model_x_disp')
odb = session.openOdb(name='x_disp.odb')
step1 = odb.steps.values()[0]
for x in odb.steps[step1.name].frames:
    odbSelectResults = x.fieldOutputs['S']
    odbSelectResults2 = x.fieldOutputs['LE']
    odbSelectResults3 = x.fieldOutputs['IVOL']
    field1 = odbSelectResults
    field2 = odbSelectResults2
    field3 = odbSelectResults3
stress11 = []
stress22 = []
stress33 = []
stress12 = []
stress13 = []
stress23 = []
strain11 = []
strain22 = []
```

```

strain33 = []
strain12 = []
strain13 = []
strain23 = []
ivol = []
result = []
#-----
for s in field1.values:
    stress11.append(s.data[0])
    stress22.append(s.data[1])
    stress33.append(s.data[2])
    stress12.append(s.data[3])
    stress13.append(s.data[4])
    stress23.append(s.data[5])
for e in field2.values:
    strain11.append(e.data[0])
    strain22.append(e.data[1])
    strain33.append(e.data[2])
    strain12.append(e.data[3])
    strain13.append(e.data[4])
    strain23.append(e.data[5])
#-----
for i in field3.values:
    ivol.append(i.data)
sumivol = []
sumivol = 0
for i in ivol:
    sumivol += i
#-----
Si11 = [(stress11[i] * ivol[i]) for i in range(len(stress11))]

```



```
Si22 = [(stress22[i] * ivol[i] for i in range(len(stress22))]  
Si33 = [(stress33[i] * ivol[i] for i in range(len(stress33))]  
Si12 = [(stress12[i] * ivol[i] for i in range(len(stress12))]  
Si13 = [(stress13[i] * ivol[i] for i in range(len(stress13))]  
Si23 = [(stress23[i] * ivol[i] for i in range(len(stress23))]  
Ei11 = [(strain11[i] * ivol[i] for i in range(len(strain11))]  
Ei22 = [(strain22[i] * ivol[i] for i in range(len(strain22))]  
Ei33 = [(strain33[i] * ivol[i] for i in range(len(strain33))]  
Ei12 = [(strain12[i] * ivol[i] for i in range(len(strain12))]  
Ei13 = [(strain13[i] * ivol[i] for i in range(len(strain13))]  
Ei23 = [(strain23[i] * ivol[i] for i in range(len(strain23))]
```

```
#-----
```

```
S_sum11 = []  
S_sum11 = 0  
for k in Si11:  
    S_sum11 += k  
S_sum22 = []  
S_sum22 = 0  
for k in Si22:  
    S_sum22 += k  
S_sum33 = []  
S_sum33 = 0  
for k in Si33:  
    S_sum33 += k  
S_sum12 = []  
S_sum12 = 0  
for k in Si12:  
    S_sum12 += k  
S_sum13 = []  
S_sum13 = 0
```

```

for k in Si13:
    S_sum13 += k
S_sum23 = []
S_sum23 = 0
for k in Si23:
    S_sum23 += k
#-----
E_sum11 = []
E_sum11 = 0
for k in Ei11:
    E_sum11 += k
E_sum22 = []
E_sum22 = 0
for k in Ei22:
    E_sum22 += k
E_sum33 = []
E_sum33 = 0
for k in Ei33:
    E_sum33 += k
E_sum12 = []
E_sum12 = 0
for k in Ei12:
    E_sum12 += k
E_sum13 = []
E_sum13 = 0
for k in Ei13:
    E_sum13 += k
E_sum23 = []
E_sum23 = 0
for k in Ei23:

```

```
E_sum23 += k
#-----
S_ave11 = S_sum11 / sumivol
S_ave22 = S_sum22 / sumivol
S_ave33 = S_sum33 / sumivol
S_ave12 = S_sum12 / sumivol
S_ave13 = S_sum13 / sumivol
S_ave23 = S_sum23 / sumivol
E_ave11 = E_sum11 / sumivol
E_ave22 = E_sum22 / sumivol
E_ave33 = E_sum33 / sumivol
E_ave12 = E_sum12 / sumivol
E_ave13 = E_sum13 / sumivol
E_ave23 = E_sum23 / sumivol
#-----
if E_ave11 == 0 :
    C11 = 0
    C21 = 0
    C31 = 0
    C41 = 0
    C51 = 0
    C61 = 0
else:
    C11 = S_ave11 / E_ave11
    C21 = S_ave22 / E_ave11
    C31 = S_ave33 / E_ave11
    C41 = S_ave12 / E_ave11
    C51 = S_ave23 / E_ave11
    C61 = S_ave13 / E_ave11
```

For shear displacements, xy displacement calculations are shown. Similar procedure is done for xz and yz displacements, too.

```
import sys
from odbAccess import *
from abaqusConstants import*
from types import IntType
import numpy as np
#openMdb('spherical_model_xy_disp')
odb = session.openOdb(name='xy_disp.odb')
step1 = odb.steps.values()[0]
for x in odb.steps[step1.name].frames:
    odbSelectResults = x.fieldOutputs['S']
    odbSelectResults2 = x.fieldOutputs['LE']
    odbSelectResults3 = x.fieldOutputs['IVOL']
    field1 = odbSelectResults
    field2 = odbSelectResults2
    field3 = odbSelectResults3
stress11 = []
stress22 = []
stress33 = []
stress12 = []
stress13 = []
stress23 = []
strain11 = []
strain22 = []
strain33 = []
strain12 = []
strain13 = []
strain23 = []
ivol = []
```

```

result = []
#-----
for s in field1.values:
    stress11.append(s.data[0])
    stress22.append(s.data[1])
    stress33.append(s.data[2])
    stress12.append(s.data[3])
    stress13.append(s.data[4])
    stress23.append(s.data[5])
#-----
for e in field2.values:
    strain11.append(e.data[0])
    strain22.append(e.data[1])
    strain33.append(e.data[2])
    strain12.append(e.data[3])
    strain13.append(e.data[4])
    strain23.append(e.data[5])
#-----
for i in field3.values:
    ivol.append(i.data)
#-----
sumivol = []
sumivol = 0
for i in ivol:
    sumivol += i
#-----
Si11 = [(stress11[i] * ivol[i]) for i in range(len(stress11))]
Si22 = [(stress22[i] * ivol[i]) for i in range(len(stress22))]
Si33 = [(stress33[i] * ivol[i]) for i in range(len(stress33))]
Si12 = [(stress12[i] * ivol[i]) for i in range(len(stress12))]

```

```

Si13 = [(stress13[i] * ivol[i]) for i in range(len(stress13))]
Si23 = [(stress23[i] * ivol[i]) for i in range(len(stress23))]
Ei11 = [(strain11[i] * ivol[i]) for i in range(len(strain11))]
Ei22 = [(strain22[i] * ivol[i]) for i in range(len(strain22))]
Ei33 = [(strain33[i] * ivol[i]) for i in range(len(strain33))]
Ei12 = [(strain12[i] * ivol[i]) for i in range(len(strain12))]
Ei13 = [(strain13[i] * ivol[i]) for i in range(len(strain13))]
Ei23 = [(strain23[i] * ivol[i]) for i in range(len(strain23))]
#-----
S_sum11 = []
S_sum11 = 0
for k in Si11:
    S_sum11 += k
S_sum22 = []
S_sum22 = 0
for k in Si22:
    S_sum22 += k
S_sum33 = []
S_sum33 = 0
for k in Si33:
    S_sum33 += k
S_sum12 = []
S_sum12 = 0
for k in Si12:
    S_sum12 += k
S_sum13 = []
S_sum13 = 0
for k in Si13:
    S_sum13 += k

```

```
S_sum23 = []  
S_sum23 = 0  
for k in Si23:  
    S_sum23 += k
```

```
#-----
```

```
E_sum11 = []  
E_sum11 = 0  
for k in Ei11:  
    E_sum11 += k
```

```
E_sum22 = []  
E_sum22 = 0  
for k in Ei22:  
    E_sum22 += k
```

```
E_sum33 = []  
E_sum33 = 0  
for k in Ei33:  
    E_sum33 += k
```

```
E_sum12 = []  
E_sum12 = 0  
for k in Ei12:  
    E_sum12 += k
```

```
E_sum13 = []  
E_sum13 = 0  
for k in Ei13:  
    E_sum13 += k
```

```
E_sum23 = []  
E_sum23 = 0  
for k in Ei23:  
    E_sum23 += k
```

```
#-----
```

```
S_ave11 = S_sum11 / sumivol
```

```
S_ave22 = S_sum22 / sumivol
```

```
S_ave33 = S_sum33 / sumivol
```

```
S_ave12 = S_sum12 / sumivol
```

```
S_ave13 = S_sum13 / sumivol
```

```
S_ave23 = S_sum23 / sumivol
```

```
E_ave11 = E_sum11 / sumivol
```

```
E_ave22 = E_sum22 / sumivol
```

```
E_ave33 = E_sum33 / sumivol
```

```
E_ave12 = E_sum12 / sumivol
```

```
E_ave13 = E_sum13 / sumivol
```

```
E_ave23 = E_sum23 / sumivol
```

```
#-----
```

```
if E_ave12 == 0 :
```

```
    C11 = 0
```

```
    C21 = 0
```

```
    C31 = 0
```

```
    C41 = 0
```

```
    C51 = 0
```

```
    C61 = 0
```

```
else:
```

```
    C14 = S_ave11 / E_ave12
```

```
    C24 = S_ave22 / E_ave12
```

```
    C34 = S_ave33 / E_ave12
```

```
    C44 = S_ave12 / E_ave12
```

```
    C54 = S_ave23 / E_ave12
```

```
    C64 = S_ave13 / E_ave12
```


B. Randomly Selected Cubes for CNT Placement

Selected cubes for CNT placement are picked by Python random algorithm.

```
import random
n=318 #input
m=1000
random_pick=random.sample(range(m), n)
#-----
import pandas as pd
data = pd.read_excel (r'C:\Temp\coordinates.xlsx')
df_x = pd.DataFrame(data, columns= ['x'])
df_y = pd.DataFrame(data, columns= ['y'])
df_z= pd.DataFrame(data, columns= ['z'])
x_coord=df_x['x'].tolist()
y_coord=df_y['y'].tolist()
z_coord=df_z['z'].tolist()
#-----
fx_csys=[]
fy_csys=[]
fz_csys=[]
for i in random_pick:
    new_x = x_coord[i] #picked x coords
    fx_csys.append(new_x)
    new_y = y_coord[i] #picked y coords
    fy_csys.append(new_y)
    new_z = z_coord[i] #picked z coords
    fz_csys.append(new_z)

print('fx_csys=',fx_csys)
```

```
print('fy_csys=',fy_csys)
print('fz_csys=',fz_csys)
```

C. Python Code for Randomly Selected Angles

CNTs have Euler angles for their placement. Euler angles of CNTs are randomly selected by using Python random algorithm.

```
import random
import numpy as np
n = 318 #input
r=90
numbers = list(range(-r,r+1))
chosen = []
for i in range(n):
    rn = random.choice(numbers)
    chosen.append(rn)
print('fiber_angle_x=',chosen)
#-----
numbers = list(range(-r,r+1))
chosen = []
for i in range(n):
    rn = random.choice(numbers)
    chosen.append(rn)
print('fiber_angle_y=',chosen)
#-----
numbers = list(range(-r,r+1))
chosen = []
for i in range(n):
    rn = random.choice(numbers)
    chosen.append(rn)
print('fiber_angle_z=',chosen)
```


D. 3x3 Cluster Model Results for 2% and 3% Volume Fraction

Results for 3x3 cluster model with 2% and 3% volume fraction are provided in Table 5.1 and Table 5.2.

Table 5.1 Homogenized elastic properties for five different 3x3 cluster models with volume fraction of 2%

sample #	1	2	3	4	5	AVG
E₁ [MPa]	7068	7166	7183	7216	6982	7123
E₂ [MPa]	7102	6993	7199	7149	7189	7126
E₃ [MPa]	7191	7120	7017	7113	7220	7132
G₁₂ [MPa]	1185	1184	1169	1170	1168	1175
G₁₃ [MPa]	1139	1122	1148	1136	1135	1136
G₂₃ [MPa]	1151	1141	1162	1154	1142	1150
v₁₂ [-]	0.29	0.28	0.28	0.28	0.28	0.28
v₁₃ [-]	0.28	0.28	0.28	0.28	0.28	0.28
v₂₃ [-]	0.28	0.28	0.29	0.28	0.28	0.28

Table 5.2 Homogenized elastic properties for five different 3x3 cluster models with volume fraction of 3%

sample #	1	2	3	4	5	AVG
E₁ [MPa]	10090	10370	10028	10283	10293	10213
E₂ [MPa]	10346	10266	10294	10388	10118	10283
E₃ [MPa]	10249	10136	10359	10140	10381	10253
G₁₂ [MPa]	1581	1559	1578	1558	1600	1575
G₁₃ [MPa]	1493	1489	1494	1506	1487	1494
G₂₃ [MPa]	1501	1485	1490	1488	1505	1494
v₁₂ [-]	0.24	0.24	0.24	0.24	0.24	0.24
v₁₃ [-]	0.23	0.24	0.24	0.24	0.24	0.24
v₂₃ [-]	0.24	0.24	0.24	0.24	0.24	0.24

Table 5.3 Comparison of elastic and shear modulus with changing volume fraction for random and 3x3 cluster model

Volume Fraction [%]	Difference in elastic modulus [%]	Difference in shear modulus [%]
1	0.83	0.26
2	0.27	-0.03
3	1.59	0.04

Mean values of the elastic and the shear moduli are compared between the 3x3 cluster model and the random model (Table 4.6, Table 4.7, Table 4.8) which has been studied before. According to the results, the difference between models can be ignored. It shows that small clusters in the model does not changing the mechanical properties of the model.